VOLATILE ORGANIC COMPOUNDS (VOC) GAS LEAK DETECTION BY USING INFRARED SENSORS

A THESIS

SUBMITTED TO THE DEPARTMENT OF ELECTRICAL AND ELECTRONICS ENGINEERING

AND THE INSTITUTE OF ENGINEERING AND SCIENCE

OF BİLKENT UNIVERSITY

IN PARTIAL FULFILLMENT OF THE REQUIREMENTS

FOR THE DEGREE OF

MASTER OF SCIENCE

By

Fatih Erden

July 2009

I certify that I have read this thesis and that in my opinion it is fully adequate, in scope and in quality, as a thesis for the degree of Master of Science.

Prof. Dr. A. Enis Çetin (Supervisor)

I certify that I have read this thesis and that in my opinion it is fully adequate, in scope and in quality, as a thesis for the degree of Master of Science.

Prof. Dr. Özgür Ulusoy

I certify that I have read this thesis and that in my opinion it is fully adequate, in scope and in quality, as a thesis for the degree of Master of Science.

Dr. Onay Urfalıoğlu

Approved for the Institute of Engineering and Sciences:

Prof. Dr. Mehmet B. Baray
Director of Institute of Engineering and Sciences

ABSTRACT

VOLATILE ORGANIC COMPOUNDS(VOC) GAS LEAK DETECTION BY USING INFRARED SENSORS

Fatih Erden

M.S. in Electrical and Electronics Engineering

Supervisor: Prof. Dr. A. Enis Çetin

July 2009

Advances in technology and industry leads to a rise in the living standards of people. However, this has also introduced a variety of serious problems, such as the undesired release of combustible and toxic gases which have become an essential part of domestic and industrial life. Therefore, detection and monitoring of VOC gases have become a major problem in recent years. In this thesis, we propose novel methods for detection and monitoring VOC gas leaks by using a Pyro-electric (or Passive) Infrared (PIR) sensor and a thermopile sensor. A continuous time analog signal is obtained for both of the sensors and sent to a PC for signal processing. While using the PIR sensor, we have Hidden Markov Models (HMM) for each type of event to be classified. Then, by using a probabilistic approach we determine which class any test signal belongs to. In the case of a thermopile sensor, in addition to Hidden Markov Modeling method, we also use a method based on the period of the sensor signal. The frequency of the output signal of the thermopile sensor increases with the presence of VOC gas leak. By using this fact, we control whether the period of a test signal is below a predefined threshold or not. If it is, our system triggers an alarm. Moreover, we present different methods to find the periods of a given signal.

Keywords: VOC gas leak detection, pyro-electric infrared (PIR) sensor, thermopile sensor, wavelet transform, Hidden Markov Models (HMM), analysis of periodic signal

ÖZET

KIZILBERİSİ ALGILAYICILARLA UÇUCU ORGANİK BİLEŞENLER KAÇAĞI TESPİTİ

Fatih Erden

Elektrik ve Elektronik Mühendisliği Bölümü Yüksek Lisans

Tez Yöneticisi: Prof. Dr. A. Enis Çetin

Temmuz 2009

Teknoloji ve endüstrideki gelişmeler, hayat standartlarını inanılmaz ölçüde artırdı. Bu gelişmeler, ev ve endüstriyel yaşamımızın vazgeçilmezi olan, aynı zamanda yanıcı ve zehirli özellikleri olan gazların açığa çıkması gibi çeşitli problemleri de beraberinde getirdi. Bu nedenle, tehlike teşkil eden gazların gözetlenmesi ve tespit edilmesi önem kazandı. Bu tezde, pyro-elektrik kızılberisi ve termopil algılaycılar kullanarak gaz tespit edilmesi için yeni metotlar önerilmiş ve uygulanmıştır. Her iki algılayıcı için de elde edilen sürekli analog sinyaller, analizi yapılmak üzere bilgisayara gönderilmektedir. PIR algılaycı sinyali analiz edilirken, sınıflandırılacak her bir olay için, saklı Markov modelleri oluşturulmaktadır. Sonrasında, olasılık yaklaşımı gözetilerek bir test sinyalinin hanig modele ait olduğu belirlenmektedir. Termopil algılayıcı durumunda ise, saklı Markov model kullanımı yanında bir de periyoda dayalı bir metot geliştirilmiştir. Termopil algılayıcı çıkış sinyalinin frekansı, ortamdaki gaz kaçağı varlığıyla artış göstermektedir. Bu durumdan hareketle, çıkış sinyalinin periyodunun daha önceden belirlenmiş bir eşik değerinin altında olup olmadığı kontrol edilmektedir. Eğer öyle ise, sistemimiz alarm üretmektedir. Bu çalışmada ayrıca periyodik bir sinyalin periyodunun bulunması için farklı metotlar sunulmaktadır.

Anahtar kelimeler: uçucu organik bileşenler kaçağı tespiti, pyro-elektrik kızılberisi algılayıcı, termopil algılayıcı, dalgacık dönüşümü, saklı Markov modelleri, periyodik sinyal analizi

Acknowledgement

I would like to express my gratitude to Prof. Dr. A. Enis Çetin for his supervision, suggestions and encouragement throughout the development of this thesis.

I am also indebted to Prof. Dr. Özgür Ulusoy and Dr. Onay Urfalıoğlu accepting to read and review this.

I wish to thank all of my friends and colleagues at Bilkent University for their collaboration and support. My special thanks go to Birey Soyer, Osman Günay and Kasım Taşdemir.

It is a great pleasure to express my special thanks to my family who brought me to this stage with their endless patience and dedication.

I would like to extend my thanks to Scientific and Technical Research Council of Turkey-TÜBİTAK for their financial support.

Contents

List of Figures

List of Tables

Chapter 1

Introduction

The current era of high technology and industrial development lead to an incredible rise in living standards. However, this has also been accompanied by a variety of serious problems, such as the undesired release of various chemical pollutants, flammable and toxic gases etc. Organic fuels and other chemicals have become an essential part of domestic as well as industrial life. Natural gas, which is a mixture of hydrocarbon gases and formed primarily of methane, ethane, propane and butane [1], is used in homes for cooking, heating and water heating. A natural gas leak can be dangerous, because it increases the risk of fire or explosion. The specific needs for VOC gas detection have emerged particularly with these improvements and the awareness of the need to protect the environment. Therefore, to prevent or minimize the damage caused by those, monitoring and controlling systems that can rapidly and reliably detect and quantify the danger are needed.

In this thesis, we study the VOC gas leak detection by using a Passive Infrared (PIR-325) Sensor and a HIS A21 F4.26 4PIN type-Heimann

Thermopile Sensor. Pyro-electric and thermopile sensors basically convert received thermal infrared power to an electrical output signal. While using conventional detectors, the VOC gas has to reach the detector to be detected. Therefore, their response time is long, especially in large rooms and they cannot be used in open areas. On the other hand, since PIR and thermal sensors operate in the infrared range of the electromagnetic spectrum and the produced output voltages depend on the amount of the absorbed infrared radiation, it is sufficient for the VOC gas to be in the viewing range of the sensors to be detected. They exhibit both good signal-to-noise performance and rapid response.

Infrared radiation exists in the electromagnetic spectrum at a wavelength longer than visible light. It cannot be seen, but can be detected. Objects that generate heat also generate infrared radiation, which is a strict function of its temperature [2]. For example, the radiation of a human body is strongest at a wavelength of 9.4 μm. Many VOC gases that we wish to detect in our environment are infrared active and exhibit bands of absorption lines in the infrared part of the spectrum, typically from 2.5 to 15 μm [3]. These absorptions provide detecting the presence of a VOC gas and measuring its concentration. Gas absorption bands are distributed across the infrared spectrum and each gas molecule absorbs radiation at characteristic wavelengths. This provides the means to distinguish one gas from another. In this work, we focus on the detection of two VOC gases: butane and propane. We use a gas cylinder that consists of 70% butane and 30% propane in our experiments. Absorption bands of butane and propane are shown in Figure 1.1. Both of the VOC gases have a peak between 3 and 4 μm bands in the infrared spectrum. PIR sensor and thermopile sensor have a spectral response of 3~14 μm and 3.26~4.31 μm, respectively. Therefore, we expect to see changes in the

output voltages of the sensors when there is a butane or propane leak in the viewing range of the sensors.

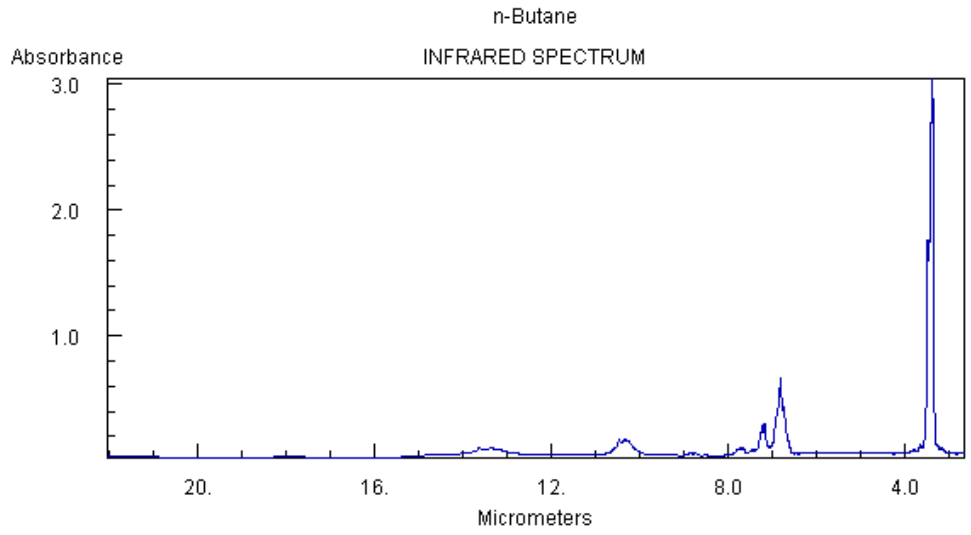

(a)

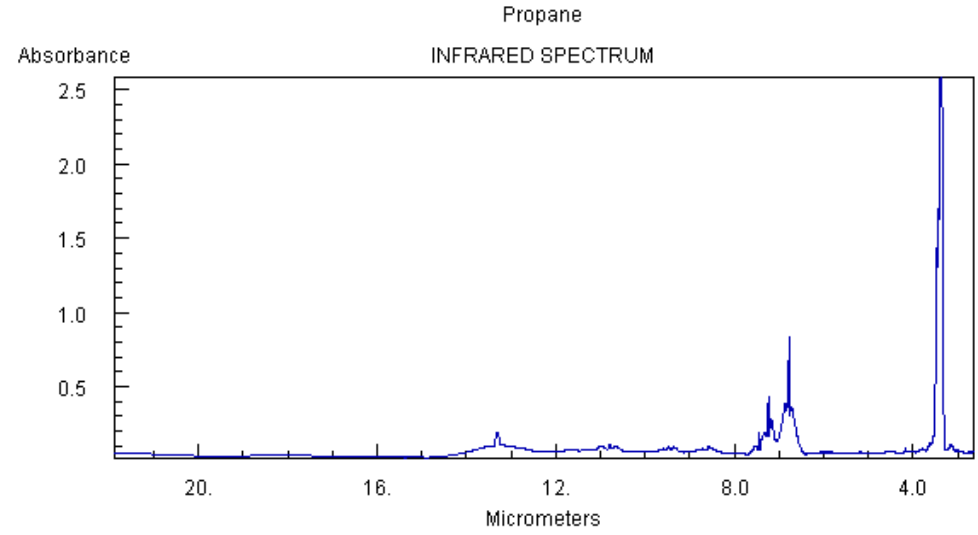

(b)

Figure 1.1 Absorption bands of (a) butane and (b) propane.

For both of the sensors, we design a circuit and obtain a continuous time analog signal for the sensor outputs. The output is send to a PC and analyzed. For sensor signal processing, we use Hidden Markov Modeling (HMM). We first generate a model for each event to be classified, i.e. no-activity, walking man and VOC gas leak events and determine which model an input signal belongs to by using a probabilistic approach. In the analysis of the thermopile sensor data, we also use a periodicity-based approach. The frequency of the sensor output signal increases with the VOC gas leak. We try to detect VOC gas leak, by controlling whether the period of an incoming signal is below a predefined threshold value.

In Chapter 2, we summarize the recent applications of infrared sensors and conventional gas detectors. We also review the flame detection method described in [4]. In Chapter 3, we describe the characteristics of a PIR sensor and a modified PIR sensor circuit designed to obtain a continuous time analog signal from the PIR sensor output. The methods for VOC gas detection by using a PIR sensor and a thermopile sensor are presented in Chapters 4 and 5, respectively. Finally, Chapter 6 concludes this thesis by providing an overall summary of all results.

Chapter 2

Related Work

In recent years, there have been several studies on pyro-electric infrared (PIR) sensors and several applications of them have been developed, such as intruder detecting, wisely light controlling, monitoring the flow in traffic, collecting people's information [5, 6], etc. PIR sensors are preferred over other sensors and cameras, mainly because of its faster response time and low-cost. Additionally, they avoid privacy, extendibility and maintenance issues. Some of the recent applications of the PIR sensors are described in Section 2.1.

There are several types of detectors commercially available, that use different detection methods, developed for gas leak. Some important ones can be summarized as [7, 8]:

- Catalytic detectors,
- Thermal conductivity sensors,
- Semi-conductors, and
- Electrochemical gas sensors.

The basic working principles and disadvantages of these sensors are explained in Section 2.2. In Section 2.3, since we use a similar algorithm based on Markov models for VOC gas leak detection, we review the flame detection method by using a pyro-electric (or passive) infrared (PIR) sensor presented by Cetin et al [4].

2.1 Recent Applications of Pyro-electric Infrared (PIR) Sensors

In [9], Tsai and Young describe a system for measurement of noncontacted temperature by monitoring an object's radiation in the infrared spectrum. They conduct using a measuring device by passing through a data acquisition and a long-term observation of the temperature variance of objects on a personal computer. The measurement mechanism consists of a PIR sensor joined with an optical chopper and Fresnel lens, where the optical chopper is put between the sensor and the lens. The proposed system can monitor the temperature of indoor equipment, especially a power substation with embedded danger, with an average error rate of 1.21% in the overall range from 40 to 200 °C. It is stated in [9] that the system provides recognizing the phenomenon of the temperature rise-rate or the critical temperature point, therefore a possible fire accident.

There are two approaches for indoor location detection systems: terminal-based and non-terminal-based method. In terminal-based method, there is a type of device that should be carried by the resident. However, non-terminal-based method requires no such device. In [10], Nam Ha et al. present a non-terminal-based method that uses an array of pyro-electric infrared sensors (PIR sensors) to detect the location of residents. The PIR sensors are placed on the

ceiling and the detection areas of adjacent sensors overlap. Then to locate a resident, the information collected from multiple sensors are integrated. The decision for the location of the resident is made due to the strength of the output analog signals collected from each PIR sensor. In the experimental test bed in a room of 4 x 4 x 2.5m (width x length x height), the system finds the location of the residence with an error smaller than 50cm, where the residents are between 160 and 180cm tall and moving at speeds between 1.5 and 2.5 km/h. Moreover, they prevent pets and other non-human moving objects from being detected by defining a threshold voltage and using a Fresnel lens, which allows only human infrared waveforms to pass through it and rejects others.

In [11], Cetin et al. propose a classification method for 5 different human motion events with one additional "no action" event by using a modified PIR Sensor. Classified events are tangential walking at 2m, tangential walking at 5m, tangential running at 5m, radial walking from a distance of 5m to the sensor and radial walking from sensor to a distance of 5m from the sensor. Classification is done by using Conditional Gaussian Mixture Models (CGMM) trained for each class. 1-D analog output signal of PIR sensor is fed into CGMM, logarithmic probabilities of the test signal is calculated according to each model and the decision is made due to the model yielding highest probability.

In [12], Lee introduces a method and apparatus for detecting direction and speed by using a dual PIR sensors in cooperation with a switch controller employing a counter and a timer. PIR sensors are aligned in a motion plane and the plurality of the sensors permit speed and direction determinations for moving IR sources by using the fact that the sensors provide different voltage outputs depending upon a relative direction of movement of an object. The switch controller controls the light. When a person enters the room, the switch turns on the lights and reset the timer. When the timer expires, the lights are

turned off. Additionally, the counter counts the number of objects entering or leaving. If the number of exits equals to number of entrances, the switch extinguishes the lights. The invention provides an energy conservative switch.

In this thesis, we also deal with a classification problem, but we focus on the detection of VOC gas leak with a PIR sensor and a thermopile sensor by using Hidden Markov Modeling and some characteristics of the output signal of the sensors (i.e., periodicity of the sensor output signal).

2.2 Gas Leak Detectors

Catalytic detector, commonly known as the "pellistor", used for combustible gases and is essentially a catalytic microcalorimeter [3]. It has a catalytic surface constructed around a temperature sensor and a heater to maintain the catalyst at a sufficiently high temperature for rapid combustion of any flammable gas molecules present. Temperature measurement and heating functions are usually combined in a platinum coil which is maintained at 500°C by a current through the wire. When the temperature increases during combustion, the resistance of the wire changes and the gas concentration is determined due to these changes [13, 14]. Therefore, catalytic sensor is not selective and its response depend on the flammable gas concentration and the rate of diffusion of the flammable gas to the sensor. There must be at least 15% oxygen (O2) concentration in the environment for the sensor to work. Moreover, the pellistor can be seriously poisoned by contaminants (e.g., lead, silicone and certain other gases) in the atmosphere, so that it cannot respond to a flammable gas and this shortens the lifetime of the sensor [7].

Thermal conductivity (TC) gas detectors operate by comparing the thermal conductivity of a sample gas with that of a reference gas, which is usually air

[7]. Since hydrogen has the highest thermal conductivity of all known gases, TC sensors are especially used to detect hydrogen [15]. There is a ”cold ” and a ”hot” element in TC sensors and heat is transferred from the hot element to the cold one via thermal conduction through the investigated gas. The power that is necessary to heat the hot element is the measure for the thermal conductivity. TC gas detectors are not very sensitive and can only be used for gases whose thermal conductivity is significantly different from air.

Semiconductor gas sensors are widely used for detection of inflammable and certain toxic gases in the air. When a specific gas enters the semiconductor gas sensor, it reacts with the oxide coating. This causes changes in the electrical conductivity due to an oxidizing reaction, i.e., a decrease in resistance between the electrodes and gas concentration is determined by measuring the resistance [16, 17]. The conductance of the device changes with the change in the atmospheric composition. Oxygen concentration, temperature and humidity and exposure to silicone, sulphur compounds may have significant effect on the sensitivity of the detector. Furthermore, after exposure to high gas concentrations, the detector may need a recovery time of several hours [7].

Electrochemical gas sensors are widely used to detect toxic gases. In general, the electrochemical sensor has two electrodes, “sensing” and “counter”, divided by an electrolyte thin coat. There is a membrane, through which the electrolyte is isolated towards the outside and is permeable to gas. When gas enters the sensor through the membrane by diffusion, oxidation reaction occurs and this causes an electrical current proportional to gas concentration. Detection of gas is made due to the current measured between the electrodes [18]. As catalytic sensors, electrochemical gas sensors sometimes suffer from poisoning and extreme hot and cold temperatures. In

addition, it is stated in [7] that the electrochemical sensors should not be used in atmospheres containing more than 25% CO_2.

Researchers from Siemens Corporate Technology have developed a laser-supported technique for measuring CO concentration [19]. It works using a laser diode which emits infrared light with a wavelength of 2.3 micrometers. If the light beam passes through carbon monoxide, the beam is attenuated at the absorption wavelength and the gas is detected by the sensor. But, there is no experimental result and it is only stated that the system can reliably measure CO at a concentration as low as 10 ppm using an optical path length of 10 centimeters.

The weakness of the conventional detectors is that the gas has to reach the sensor in order to be detected. Therefore, conventional detectors cannot provide quick responses in large areas and cannot be utilized in open areas. On the other hand, PIR and thermopile sensors can be used both in large and open areas. Since they generate a voltage proportional to the incident infrared radiation power, it is sufficient for the VOC gas to be in the viewing range of the sensors. Other advantages of the thermopile and PIR sensors can be summarized as follows:

- Instantaneous response time,
- no poisoning,
- no need of oxygen, and
- low-cost.

2.3 Flame Detection System Based on Wavelet Analysis of PIR Sensor Signals With An HMM Decision Mechanism

In [4], a flame detection method with a PIR sensor by using an HMM decision mechanism is described. There are three types of events to be classified by using HMMs: a walking person, no-activity and flame. A model for each class is trained using past data. In this probabilistic approach, the test signal is classified according to the model for which HMMs produce the highest probability.

For VOC gas leak detection, we use a similar method to one in [4]. In this section, we review the flame detection method. We give a brief description of Hidden Markov Models in Section 2.3.1. The details of the flame detection procedure is described in Section 2.3.2.

2.3.1 Hidden Markov Models (HMM)

HMMs are commonly used in many real world applications to solve pattern recognition problems, e.g., speech recognition, gesture recognition. A Markov process is any process in which the current state depends only on the previous N states of the sequence [20]. For example, the sequence of a simple set of traffic lights (red-green-amber-repeat) represents a first order Markov process. But from a modeling perspective, stochastic processes are more interesting than deterministic processes. For example, the weather is a stochastic process. However the states of the model are usually not directly observable. This is where HMM finds its application. An HMM is a doubly stochastic process in

which the underlying states are hidden, and probabilistically related to a sequence of observed symbols [21]. A simplified example is described in [22] to understand HMM more. You are in a cave by the ocean and never see outside. You want to know what the weather is like and the only clue is a piece of seaweed that you can see from the entrance of the cave. The seaweed can be dry, dampish or wet depending on the weather. This scenario can be modeled by an HMM, where the weather is a set of hidden states and the condition of the seaweed is an observable symbol.

In [4], there are two classes: one represents fire events and the second represents non-fire events, i.e., background (no activity), walking, running, hands waving etc. It is stated that the flames of an uncontrolled fire flicker with a frequency of around 10 Hz. Recently developed fire detection schemes that are based on video, uses this fact and detects the periodic high-frequency behavior in moving pixels of flame color. But flame flicker covers a wide-band range 1 Hz to 13 Hz. Therefore, Markov modeling takes advantage of producing more robust performance over frequency domain based methods.

2.3.2 Sensor Signal Processing

In [4], a modified PIR sensor circuit is developed to capture a continuous time analog signal that represents the strength of the received signal in time. The analog signal is sampled with a sampling frequency of f_s=50 Hz. The sampling frequency is sufficient, because it is above the highest flame flicker frequency (which is 13 Hz). Having the continuous analog signal, the signal is digitized by using an analog to digital converter circuit and sent to a PC.

First, a wavelet transform takes place on the sensor output signal. Wavelet transform provide robustness against sensor signal drift due to temperature

variations in the area of interest. Since temperature changes are slow variations compared to moving objects and flames and wavelet signals are high-pass and band-pass signals, signals are not affected by the slow variations, corresponding to temperature variations. The wavelet coefficients for the output signal, $w[k]$, are obtained after high-pass filtering followed by decimation. The high pass filter, $H(z)$ has the following transfer function:

$$H(z) = \frac{1}{2} - \frac{1}{4}(z^{-1} + z^{1}) \tag{2.1}$$

Having the wavelet coefficients, an HMM based classification is carried out. Two three-state Markov models are used, one for fire and the other for walking action for a person. Two threshold values are defined for each model in the wavelet domain, T_1 and T_2, where the thresholds are non-negative. Let the states be S_1, S_2 and S_3 and $|w[k]|$ represent the absolute value of the wavelet coefficients. If $|w[k]| < T_1$, then state S_1; if $T_1 < |w[k]| < T_2$, then state S_2; if $|w[k]| > T_2$, then state S_3 is attained. In the Markov models defined, S_1 represents no activity case. As long as there is no activity in the viewing range of the PIR sensor, the system remains in S_1.

In the first step of the HMM based analysis, the wavelet coefficient sequences are divided in windows of 25 samples. Further, the corresponding state transition sequence is determined for each window. An example state transition sequence of size 5 may look like

$$C = \{S_2, S_2, S_1, S_3, S_1\}. \tag{2.2}$$

The wavelet signal captures the high frequency information in the signal. Therefore, it is expected to see more transitions between states in the case of fire compared to walking event of a person.

The thresholds, T_1 and T_2 determine the states and the state transition probabilities of a given signal. Optimum value of the thresholds are defined in the training step by using a Genetic Algorithm (GA). Having the reference signals for each class and the threshold values, transition probabilities of the classes are calculated. The state transition probabilities for a walking person and fire are estimated from 250 consecutive wavelet coefficients covering a 10 seconds time. Let a_{ij} denote the transition probabilities for fire, b_{ij} denote the transition probabilities for a walking person and C denote a state transition sequence to be tested of size L. To decide which class that C belongs to, two joint probabilities $P_a(C)$ and $P_b(C)$ (corresponding to fire and walking person classes, respectively) are calculated:

$$P_a(C) = \prod_i p_a(C_{i+1} \mid C_i) = \prod_i a_{C_i, C_{i+1}} \tag{2.3}$$

and

$$P_b(c) = \prod_i p_b(C_{i+1} \mid C_i) = \prod_i b_{C_i, C_{i+1}} \tag{2.4}$$

where i=1, …, L. The state transition sequence C belongs to 'fire' class, if $P_a(C)>P_b(C)$, otherwise it belongs to 'walking person' class. The state diagram and the definitions of the state transitions are presented in Figure 2.1.

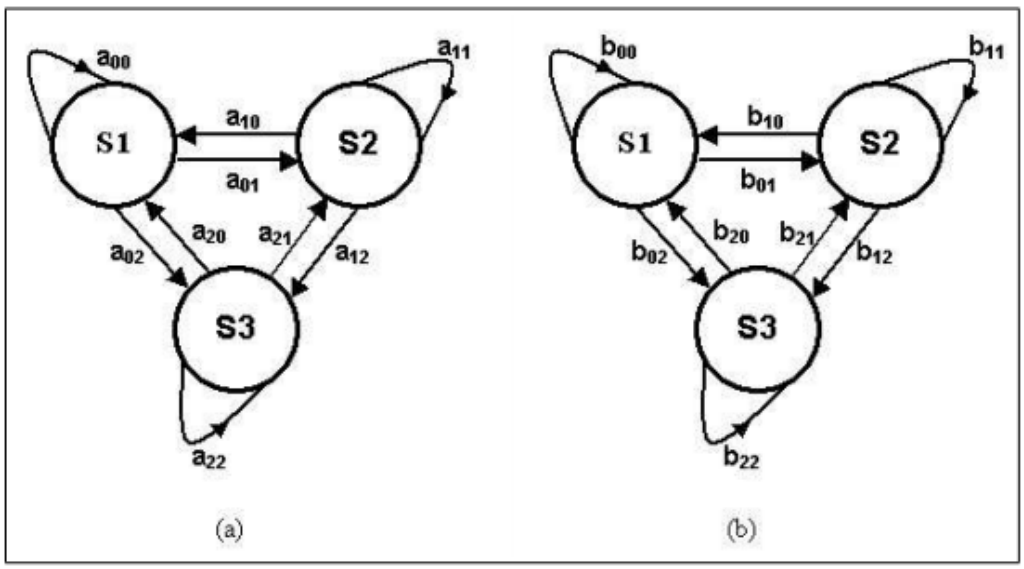

Figure 2.1: State diagram and the definitions for the state transitions for (a) 'fire' and (b) 'walking person' classes

During classification, each 50 consecutive wavelet coefficients are computed from the received PIR sensor signal and fed into 'fire' and 'walking person' models. The result of the analysis is monitored as the model yielding the higher probability.

Chapter 3

Properties of PIR Sensor and Analog Signal Processing

Passive Infrared Sensor (PIR) based system has the detection ability to monitor large rooms and spaces, because PIR sensors analyze the infrared light reflected from hot objects to make a decision. Pyro-electric sensors give an electric response to not the temperature itself, but the rate of change in the temperature. When there is a hot body motion in the viewing range of the sensor, the strength of the received signal from the PIR sensor increases.

In Section 3.1, we introduce the characteristics of a PIR sensor. Section 3.2 describes the modified PIR sensor circuit developed in [4], which we also use for VOC gas detection.

3.1 Characteristics of the PIR Device

Pyro-electric detectors are crystal devices. The crystalline material in the PIR sensor, generates a surface electric charge when it is heated by infrared radiation. The amount of this charge changes with the amount of radiation striking the crystalline material. Infrared radiation is absorbed by a coating on the crystal surface and converted to heat. The heat alters the lattice spacing of the crystal and causes a charge differential between the surfaces [6, 23]. This charge differential is measured as an output voltage.

The PIR325 sensor has two sensing elements in connection with a voltage bucking configuration. Signals caused by vibration, temperature changes and sunlight are cancelled by this arrangement. When a body passes in front of the sensor, it will activate the first sensing element and then the second one, as shown in Figure 3.1. However, other sources will affect both of the elements simultaneously and be cancelled.

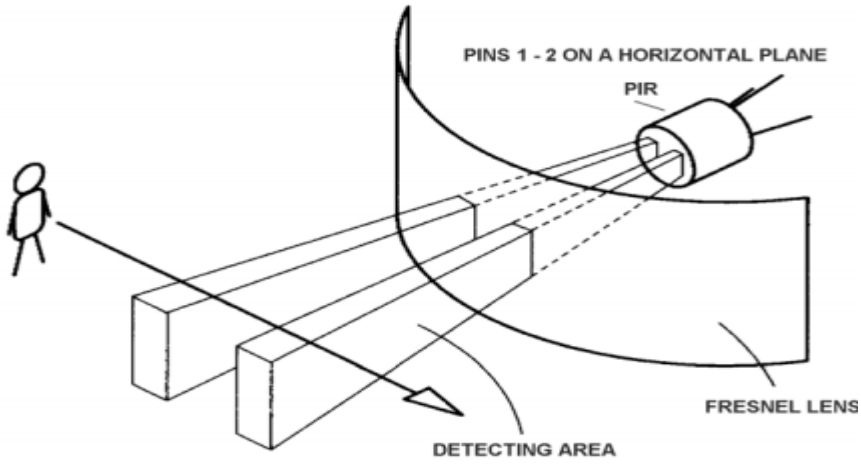

Figure 3.1: A moving body activates each sensing element in turn (taken from [23]).

The PIR325 sensor has a spectral response of 3~14 μm. The commercially available PIR sensors generally have Fresnel lens on them, as shown in Figure 4.1, to change the transmission range of the radiation. The PIR325 sensor has FL65-type lens on it, which is made of an infrared transmitting material that has an IR transmission range of 8 to 14 μm, in order to be more sensitive to radiation of human body. But, many gases that we wish to detect in our environment exhibit bands of absorption line in the infrared part of the spectrum, from 2.5 to 15 μm (especially 2.5 to 5 μm). Therefore, in this thesis the Fresnel lens is demounted and PIR325 sensor is used without a lens to be able to detect VOC gas leaks.

3.2 Modified PIR Sensor System and Data Acquisition

Commercial PIR sensor circuits produce binary outputs. To process the sensor signal, a continuous time analog signal is needed. A circuit is developed for this aim in [4] and shown in Figure 3.2. The circuit captures a continuous time analog signal that represents the strength of the received signal in time.

The circuit contains 4 low cost LM324 operational amplifiers (op amps), U1A, U1B, U1C and U1D. Amplifiers U1A and U1B, have a gain of 100, together form a two stage amplifier circuit, whereas the op amps U1C and U1D form a window comparator that responds to signals about 200 millivolts above and below Vcc/2, where Vcc is 5 V. The two stage amplifier circuit is used to amplify the very-low amplitude raw output at the 2nd pin of the PIR sensor. The amplified output signal of U1B is fed into the comparator structure. The comparator part of the circuit, outputs a binary signal, either 0 V or 5 V. The analog output signal is measured at the output of U1B, instead of using the

binary output of the original PIR sensor circuit. Then, the analog output is digitized by using a PIC16F877A-type microcontroller device as an analog to digital converter and sent to the computer via an RS-232 to USB converter. Finally, the output signal received from the USB port is read from HyperTerminal application and saved into a text file to be processed.

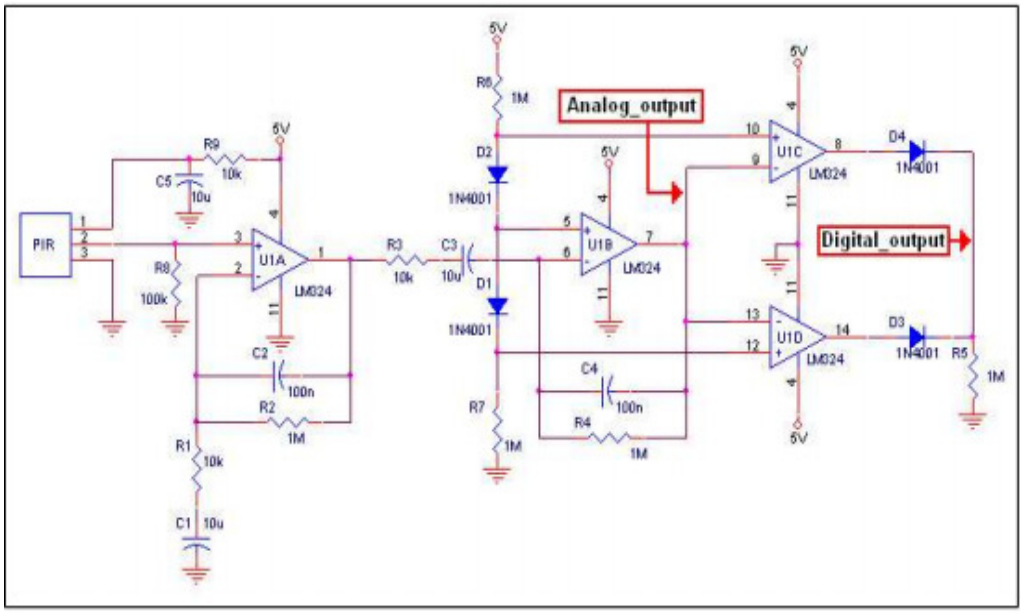

Figure 3.2: The circuit diagram of the modified PIR sensor circuit for capturing an analog signal

For VOC gas detection, the analog signal is sampled with a sampling frequency of f_s=100 Hz, which is sufficiently fast to capture a VOC gas leak. Typical sampled signal for no activity case using 8 bit quantization is presented in Figure 3.3. The value of the output signal for no activity case changes between 100 and 150. The x-axis represents the number of samples and since the sampling frequency of the output signal is 100 Hz, a time domain analysis can be obtained by dividing each number in the x-axis by 100. Figure 3.4 shows the PIR output signal due to a walking person and a gas leak event at a

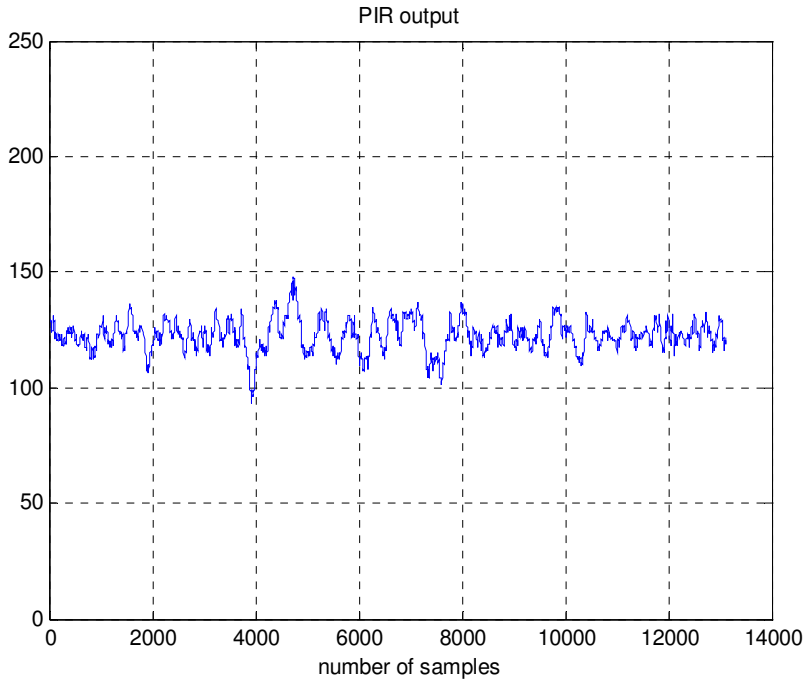

Figure 3.3: A typical PIR sensor output sampled at 100 Hz with 8 bit quantization when there is no activity in its viewing range.

distance of 1 m. In Figure 3.4 (a), there is no activity up to 33rd second and there is a walking person in the viewing range of the PIR sensor between seconds 33-40. There is no activity again up to 87th second and there is another walking event. In Figure 3.4 (b), a VOC gas leak at 53rd second is presented, after a no activity event. VOC gas leak event actually continues up to the end of the record, but after some time the observed output signal behaves as it belongs to no activity event. Because, PIR sensor circuit updates its background when the same event in its viewing range lasts for some time. In fact, this is due to the fact that the strength of the signal received from PIR sensor changes with the motion of a hot body and pyro-electric sensors give an electric response to a rate of change of temperature rather than temperature itself.

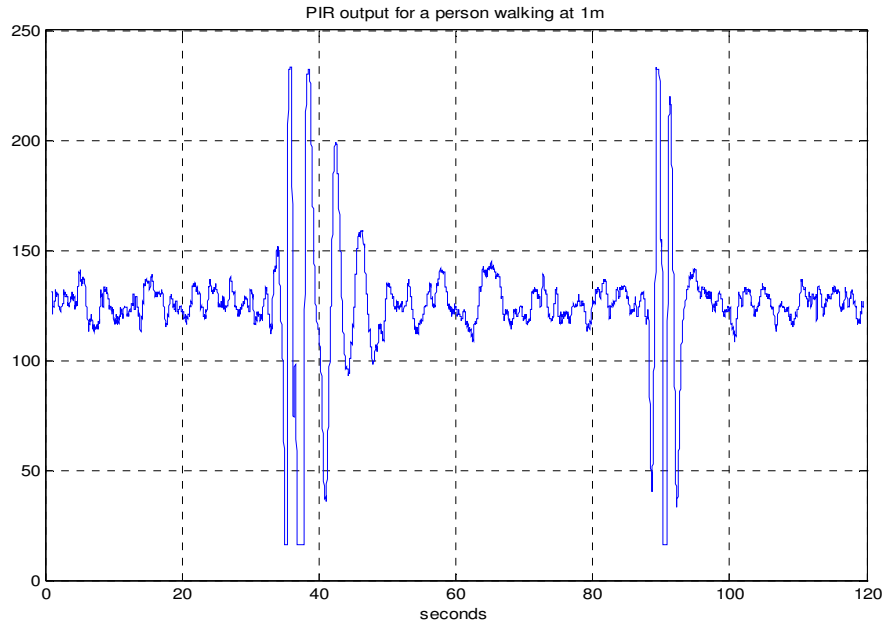

(a)

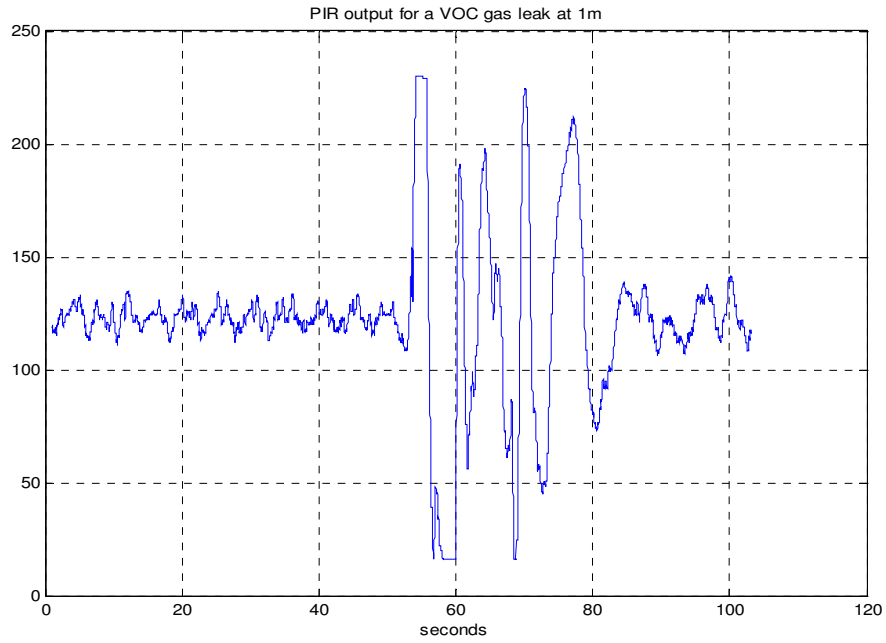

(b)

Figure 3.4: PIR sensor output signals recorded at a distance of 1m for (a) a walking person and (b) for a VOC gas leak. Sampling frequency is 100 Hz.

Chapter 4

Detection of VOC Gas Leak by Using A Pyro-electric Infrared (PIR) Sensor

In this chapter, a VOC gas leak detection system based on a pyro-electric (or passive) infrared sensor is described. Digitized PIR sensor data is analyzed by using HMMs. There are three events of interest of classification: 'no-activity', 'walking person' and 'gas leak' classes. A Markov model for each class is created and the test signal is classified using the Markov models. The wavelet coefficients are used as feature parameters by Markov models. Section 4.1 describes the HMM-based decision process of which class a test signal belongs to. Experimental results are presented in Section 4.2.

4.1 Sensor Data Processing

The strength of the PIR sensor output signal increases or decreases due to hot body actions in its viewing range and the analysis is made by using these changes. Therefore, any changes in the temperature of the room, where PIR sensor is placed, affect the analysis. Average temperature changes cause a bias in the output of the sensor. To remove this bias, wavelet transform is used. Wavelet transform is a very popular transform and used in analysis, denoising and compression of signals and images [24].

The procedure to obtain the wavelet coefficients is described in Section 4.1.1. How HMMs are applied on the wavelet domain and the way to decide which class any test signal belongs to is presented in Section 4.1.2.

4.1.1 Wavelet Transform

Let $x[n]$ be a sampled version of the signal coming out of the PIR sensor and $w[k]$ be the wavelet coefficients, which are obtained after a subband decomposition process, followed by a dyadic decimation, where k and n are integers. The filter bank of a Haar wavelet transform is used in the analysis, which is the same as a single stage Daubechies wavelet [25]. The lowpass and the highpass filter coefficients of the filter bank are, respectively:

$$h[n] = \{1, 1\} \tag{4.1}$$

and

$$g[n] = \{1, -1\} \tag{4.2}$$

The Discrete Wavelet Transform (DWT) is computed by successive low pass and high pass filtering of the discrete time-domain signal as shown in Figure 4.1. In the figure, the low pass filter is denoted by G_0 ,while the high pass filter is denoted by H_0. At each level the high pass filter produces detail information, $d[n]$, while the low pass filter associated with scaling function produces coarse approximations, $a[n]$. In this scheme, wavelet coefficients $w[k]$, are represented by $d_4[n]$. In this analysis, a four-stage decomposition is used to obtain the wavelet coefficients. Because the significant changes, which occur in the case of a VOC gas leak and a walking action of a person, are visible only at the end of the fourth stage. The wavelet coefficients for the VOC gas leak in Figure 3.4(b) is shown in Figure 4.2.

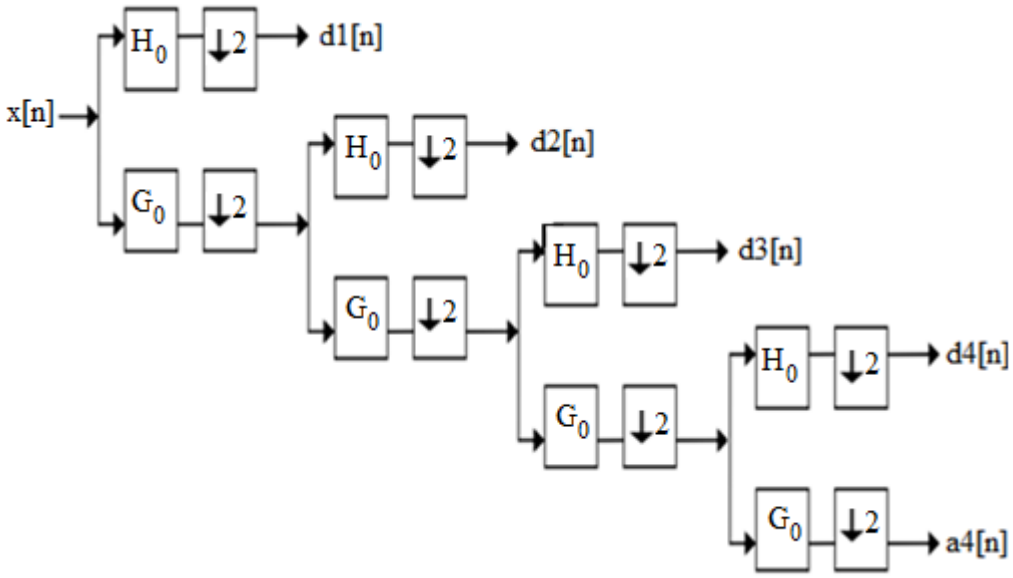

Figure 4.1: Four-level wavelet decomposition tree

At each decomposition level, the half band filters produce signals that span only half the frequency band. This doubles the frequency resolution and decimation by 2 halves the time resolution. Therefore, while the half band low

pass filtering removes the half of the frequencies and so halves the resolution, the decimation by 2 doubles the scale.

While each 100 samples correspond to 1 second in the original data, in wavelet domain each 100 samples correspond to 16 seconds.

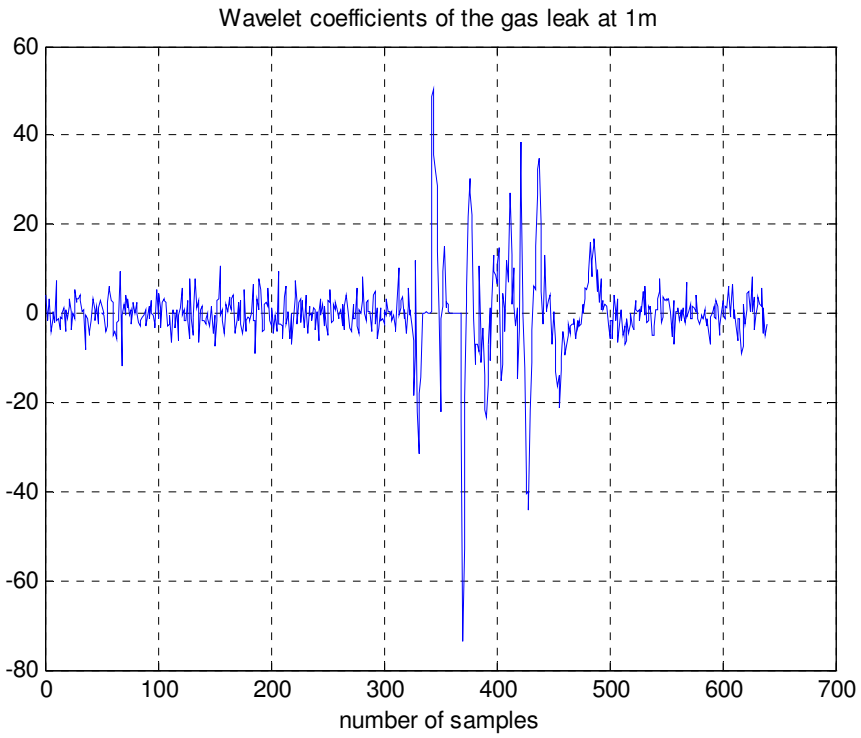

Figure 4.2: Wavelet coefficients of the PIR sensor output signal recorded at a distance of 1m for the VOC gas leak (shown in Figure 4.4(b))

4.1.2 Hidden Markov Modeling

Once the wavelet coefficients are obtained with the procedure described in Section 4.1.1, an HMM based classification, similar to one in [4], is carried out for VOC gas leak detection. There are three types of event to be classified: a walking person, a gas leak and a no-activity event. Two three-state Markov

models are used to model a VOC gas leak and a walking person. In the training step, two threshold values are defined in the wavelet domain for each model, T_1 and T_2, where T_1 is negative and T_2 is positive. The same threshold values are used in each model. Let the three states be S_0, S_1 and S_2. States of the wavelet coefficients are defined according to the algorithm implemented as follows:

```
if ( w(k) < T1 )
    then state S0,
else if (T1 < w(k) < T2 )
    then state S1,
else
    state S2 is attained accordingly.
end
```

Figure 4.3: The algorithm for state definitions of the wavelet coefficients

Thresholds are defined such that the wavelet coefficients of the no-activity event remain in state S_1. The system is in state S_1 as long as there is not any significant activity in the viewing range of the PIR sensor. Therefore, although there are three events to be classified, only two Markov models are used, one for a walking person and the other for a gas leak. No-activity event is detected by controlling whether the system remains in S_1 or not.

Once thresholds and states are defined, the next step while applying HMMs is to find the state transition sequences for predetermined reference signals of a VOC gas leak and a walking person. Let C_r be the state sequence of a reference signal. An example state sequence of size 7 may look like

$$C_r = (S_0\ S_0\ S_1\ S_2\ S_2\ S_1\ S_0) \tag{4.3}$$

Equation (4.3) shows that the first and the second wavelet coefficients of the reference signal are below the threshold T_1, the third coefficient is between T_1 and T_2 and so on. The state sequence is generated from the related part of the signal, i.e. over the part that the VOC gas leak starts and ends for the 'gas leak' class and the part when there is a walking person in the viewing range of the sensor for 'walking person' class. Let a_{ij} and b_{ij} be the number of transitions from state i to j in the state sequences of the reference signals for the 'gas leak' and the 'walking person' classes respectively and they can be defined as:

$$a=(a_{00}\ a_{01}\ a_{02}\ a_{10}\ a_{11}\ a_{12}\ a_{20}\ a_{21}\ a_{22}) \tag{4.4}$$

$$b=(b_{00}\ b_{01}\ b_{02}\ b_{10}\ b_{11}\ b_{12}\ b_{20}\ b_{21}\ b_{22}) \tag{4.5}$$

where a_{00} and b_{00} denote the number of transitions from state S_0 to S_0, a_{01} and b_{01} denotes the number of transitions from state S_0 to S_1 and so on. States and the transitions are demonstrated in Figure 4.4.

Having determined the number of transitions between the states for each reference signals, the probabilities for each transition to occur are computed. Let the lengths of the reference signals for 'gas leak' and 'walking person' classes be L_1 and L_2, respectively. Then the probability for each transition to occur is:

$$p_a(i,j) = \frac{1}{L_1} a_{ij} \tag{4.6}$$

and

$$p_b(i,j) = \frac{1}{L_2} b_{ij} \tag{4.7}$$

for the 'gas leak' and 'walking person' classes respectively, where $p_a\ (i,j)$ denotes the probability of moving from state i to state j. For the training of the HMMs, the state transition probabilities are estimated from 50 consecutive wavelet coefficients covering a time frame of 8 seconds. Training step ends up by obtaining the probabilities for each transition.

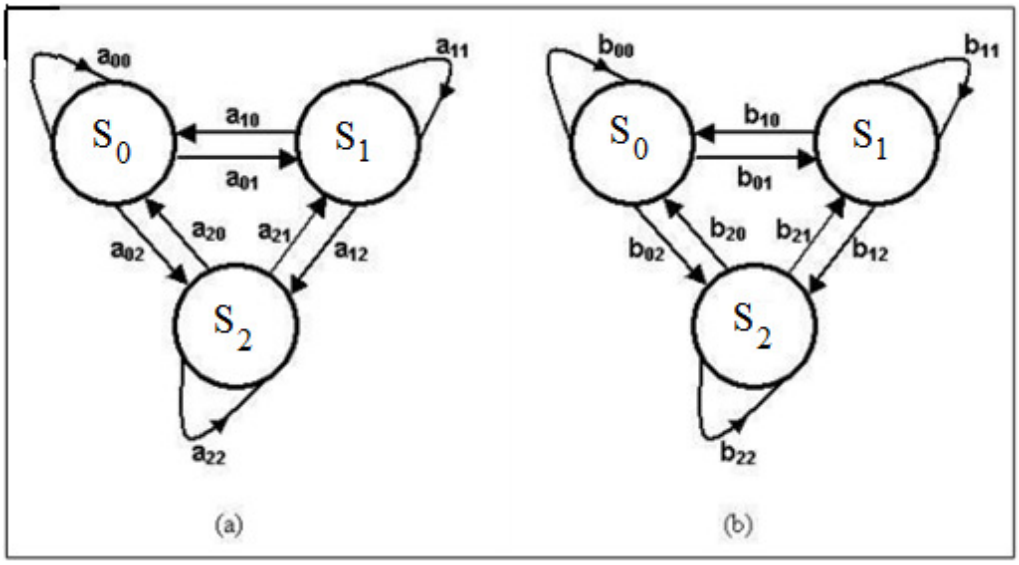

Figure 4.4: State transition definitions for (a) 'VOC gas leak' and (b) 'walking person' classes

In the classification process of the classes with HMMs, we only deal with the VOC gas leak and walking person events. Since the system remains in state S1 when there is no activity, the 5th element of the state transition probability sequence of the no-activity class, $p(1,1)$, is very close to 1 and others are very close to 0. Consequently, no-activity event is detected by first defining a threshold value close to 1 and controlling whether $p(1,1)$ of the test signal state sequence is above this threshold, without using any extra model.

To decide the class affiliation of a test signal, state vector and accordingly the number of transitions of the signal are generated first. Let C be the state

sequence of the test signal and t_{ij} be the number of transitions from i-th state to j-th state. Then the probabilities for the state sequence C of belonging to 'gas leak' and 'walking person' classes are, respectively:

$$P_a(C) = \prod_{i=1}^{L} p_a(C_{i+1} \mid C_i) = \prod_{i=0}^{2}\prod_{j=0}^{2} (p_a(i,j))^{t_{ij}} \tag{4.8}$$

and

$$P_b(C) = \prod_{i=1}^{L} p_b(C_{i+1} \mid C_i) = \prod_{i=0}^{2}\prod_{j=0}^{2} (p_b(i,j))^{t_{ij}} \tag{4.9}$$

where L is the length of the state sequence C of the test signal.

During the classification phase, the state sequence of the test signal C is divided into windows of length 25 and each window is fed into 'gas leak' and 'walking person' models. The model yielding the highest probability is determined and monitored at the end of each 4 seconds period, as the result of the analysis of PIR sensor data. To minimize the complexity of operation during classification, we use equations (4.10) and (4.11) to determine the probabilities, instead of (4.8) and (4.9). Figure 4.5 describes the algorithm implemented to decide the result.

$$P_a(C)' = \sum_{i=0}^{2}\sum_{j=0}^{2} t_{ij} \log_{10}(p_a(i,j)) \tag{4.10}$$

$$P_b(C)' = \sum_{i=0}^{2}\sum_{j=0}^{2} t_{ij} \log_{10}(p_b(i,j)) \tag{4.11}$$

if $P_a(C) > P_b(C)$

then the window affiliates to the ‘gas leak’ class

else

the window affiliates to the ‘walking person’ class

end

if $p_{test}(1,1) > 0.8$

the window affiliates to the ‘no-activity’ class

end

Figure 4.5: The algorithm to decide the class affiliation of a window of the test state sequence *C*

As an alternative way, we try two two-state Markov models to represent ‘VOC gas leak’ and ‘walking person’ models. Since there are two states, only one threshold, *T*, is sufficient and it is defined as 2σ and 3σ, where σ is the standard deviation of the sensor output signal for no-activity event. Figure 4.6 shows the two-state Markov models and the state definitions. If $w(k) < T$, then S_0 is attained, otherwise S_1 is attained. Greater than 90% of the wavelet coefficients of the signal for no-activity event remain is state S_0. Therefore, the probability of the system to remain in S_0 is greater than 0.9 and a no-activity event can be classified by controlling this probability without generating an extra Markov model.

When $T = 2\sigma$, the system triggers an alarm at each time there is a walking person or waving arm movements and when $T = 3\sigma$, all the gas leaks are considered as a walking person event. When threshold is defined between 2σ and 3σ, the system can detect some of the gas leaks but, it may analyze a walking person event as a gas leak. As a result, three-state Markov models produce better results than the two-state models.

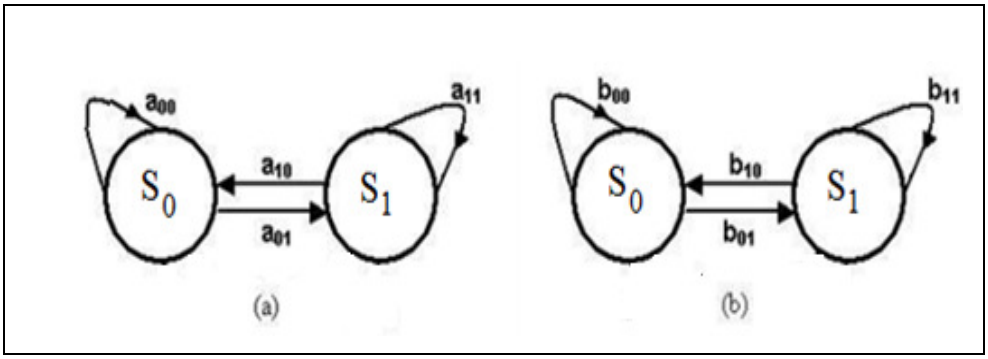

Figure 4.6: Two state Markov models for (a) 'VOC gas leak' and (b) 'walking person' classes

4.2 Experimental Results

The analog output signal is sampled with a sampling frequency of 100 Hz and quantized at 8 bits. Analysis and classification methods are implemented with MATLAB running on a PC. Digitized output signal is fed to the PC via RS-232 serial port.

The detection range of a PIR sensor based system is 5 meters, but in our experiments we record VOC gas leak and walking person sequences at a distance of up to 3 meters. Since we use the PIR sensor without the Fresnel lens on it, after 3 meters the strength of the PIR output signal decreases and the sensor is not able to response to the changes.

For the VOC gas leak records, we use a bottled gas which contains a mixture of butane and propane gases, in ratios %70 and %30 respectively and three types of experiments are hold:

- We record the VOC gas leak when it is very close and at a distance of 1m and 3 meters to the sensor. We first start the VOC gas leak, leave the viewing range of the sensor, wait until the response to a walking person disappears and then start recording.
- We use 1m-length pipe between the sensor and the bottled gas. We start recording the background and then start the VOC gas leak while recording continues.
- We first start recording the background and then start the VOC gas leak without entering the viewing range of the sensor.

The first type of experiments are uncontrolled, while the others are controlled.

For walking person sequences, we record a person walking in the viewing range of the PIR sensor on a straight line which is tangent to a circle with a radius of 1m, 2 and 3 meters and the sensor being at the center. We also record waving arm movements at distances of 1m, 2 and 3 meters to the sensor. Moreover, we record the response of the PIR sensor to air coming out of a hairdryer to test whether it will be considered as a gas leak or not. The second setup described above used in hairdryer experiments. PIR sensor output for hairdryer is shown in Figure 4.7.

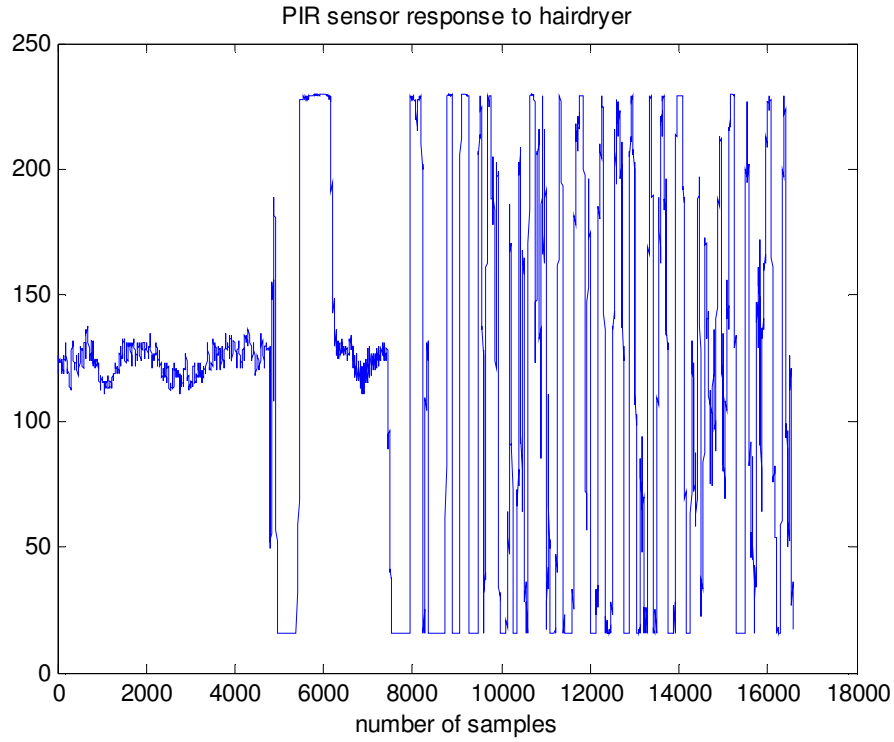

Figure 4.7: PIR sensor response to hairdryer at a distance of 1m from the sensor

In the HMM-based analysis of the PIR sensor output signal, we use the same model to test each test sequence. We also use the same threshold values, ($T_1 = -10, T_2 = +10$) to produce the reference transition probabilities and the transition numbers for the test signals. The state sequence is divided into windows of lengths 25, each covering a time frame of 4 seconds. At the end of each time frame, the result of the analysis is monitored and hold. If two consequent frames are analyzed as gas leak, we trigger an alarm. Moreover, if the probability of a transition from S_1 to S_1 to occur is greater than 0.8, we decide there is no-activity.

The response to a hairdryer, shown in Figure 4.7, is similar to the response to VOC gas leak and a walking man, but the oscillations do not die down. In the case of a VOC gas leak, PIR sensor updates its background after some time

and the sensor output signal behaves as there is no activity even if there is a gas leak. Therefore, if the analysis of 10 consecutive windows are concluded in VOC gas leak or walking man, then the alarm is turned on. The results for the HMM analysis are presented in Table 4.1.

	No. of test sequences	No. of False Alarms	No. of Missed Leaks	No. of Alarms
Gas leak test sequences	32	-	2	30
Non-gas test sequences	50	5	-	5

Table 4.1 Classification results for 32 VOC gas leak and 50 non-gas test sequences. The system triggers an alarm when a VOC gas leak is detected in the viewing range of the PIR sensor.

Our method successfully detects VOC gas leak for 30 of the 32 gas leak test sequences. The two missed leaks belong to leaks that are at a distance greater than 3 meters to the sensor. The strength of the output signal of the PIR sensor decreases for the leaks far away from the sensor and they are analyzed as a no-activity event. Our system triggers a false alarm for 5of 50 non-gas test sequences. Three of them belong to the walking person and two of them belong to the waving arm movement experiments. If a person is at a distance of up to 1m, there is no problem. But, when the person is far away, the strength of the sensor output signal decreases, as a result walking event may be confused as gas leak.

Chapter 5

Detection of VOC Gas Leak by Using A Thermopile Sensor

In this chapter, a thermopile sensor based VOC gas leak detection method is described. Thermopile sensor output signal changes due to the absorption of infrared radiation in its viewing range. A circuit is designed to process the sensor signal in PC. Sensor output signal is analyzed by using HMMs in wavelet domain and using the periodicity of the signal and determined which class, 'gas leak' or 'no-activity', it belongs to.

In Section 5.1, we introduce the properties of the thermopile device. Section 5.2 describes the circuit designed for sending the sensor data to PC. In Section 5.3, we review the method in [26], which we use to detect the periodic behavior of a signal. Sensor output signal analysis is made in Sections 5.4 and 5.5 and the experimental results are presented in Section 5.6.

5.1 Characteristics of the Thermopile Sensor

A thermopile is an electronic device that converts thermal energy into electrical energy. It measures the increase in temperature caused by the absorption of radiation [27]. It is composed of a serially-interconnected array of thermocouples, each of which consists of two dissimilar materials with a large thermoelectric power and opposite polarities. The thermocouples are placed across the hot and cold regions of a structure. The hot junctions are thermally isolated from the cold junctions. To provide effective heat sink, the cold junctions are placed on the silicon substrate. In the hot region of the sensor a black infrared radiation absorbing coating is applied. This absorbs the radiation and transduces it into heat. The heat causes temperature differences across the thermopile, which thus gives an output according to the intensity of the incident infrared light [28].

Heimann HIS A21 F4.26 4PIN type thermopile sensor has a spectral response of 3.26-4.31 µm [29]. Gases that have a characteristic absorption peak in this infrared band are sensed by the sensor. When infrared radiation passes through the gas, light energy is absorbed by its molecules. The base equation for gas concentration measurement in the infrared way is the Lambert-Beer law [30]:

$$I = I_0 \exp(-KCL) \tag{5.1}$$

where I_0 and I, denote the light intensity of infrared parallel light before and after passing the gas to be measured respectively; K denotes the absorption coefficient of gas, C denotes the gas concentration and L denotes the measuring distance.

The thermopile sensor has two output channels. One is the active channel and the other is the reference channel. Output signal of the active channel is

proportional to the light intensity and the gas concentration, whereas the reference channel output does not relate to the gas to be measured and is proportional to the light intensity too. Both output signals are proportional to light intensity and *K* and *L* are fixed for a sensor. Therefore, two scale factors, K1 and K2, can be estimated for two channels and consequently, the output signals can be defined as:

$$U_1 = K_1 I_0 \exp(-KCL), \tag{5.2}$$

and

$$U_2 = K_2 I_0 \tag{5.3}$$

for the active channel and the reference channel, respectively. The peak-to-peak voltage of the active channel lessens with the light energy absorbed by the gas molecules.

5.2 Modified Thermopile Sensor System and Data Acquisition

The active channel of the thermopile sensor is used for sensor signal processing. The circuit shown in Figure 5.1 is constructed to obtain a continuous time analog signal. It contains two LM324 operational amplifiers, U1A and U1B. U1A is used to amplify the very-low amplitude output at the 4th pin of the thermopile sensor and the output is read from the unity gain amplifier, U1B. R1-C1 couple is used to filter the noise. R3 resistor limits the current which must be in 1-2 mA range. The sensor pins are configured as in Table 5.1.

Pin No.	Symbol	Description
1	VDD	Positive supply voltage (+5V)
2	VSS	Ground (0V)
3	AOR	Analog temperature reference output voltage
4	AOT	Analog sensor output voltage

Table 5.1: Pin / Device configuration for the thermopile sensor

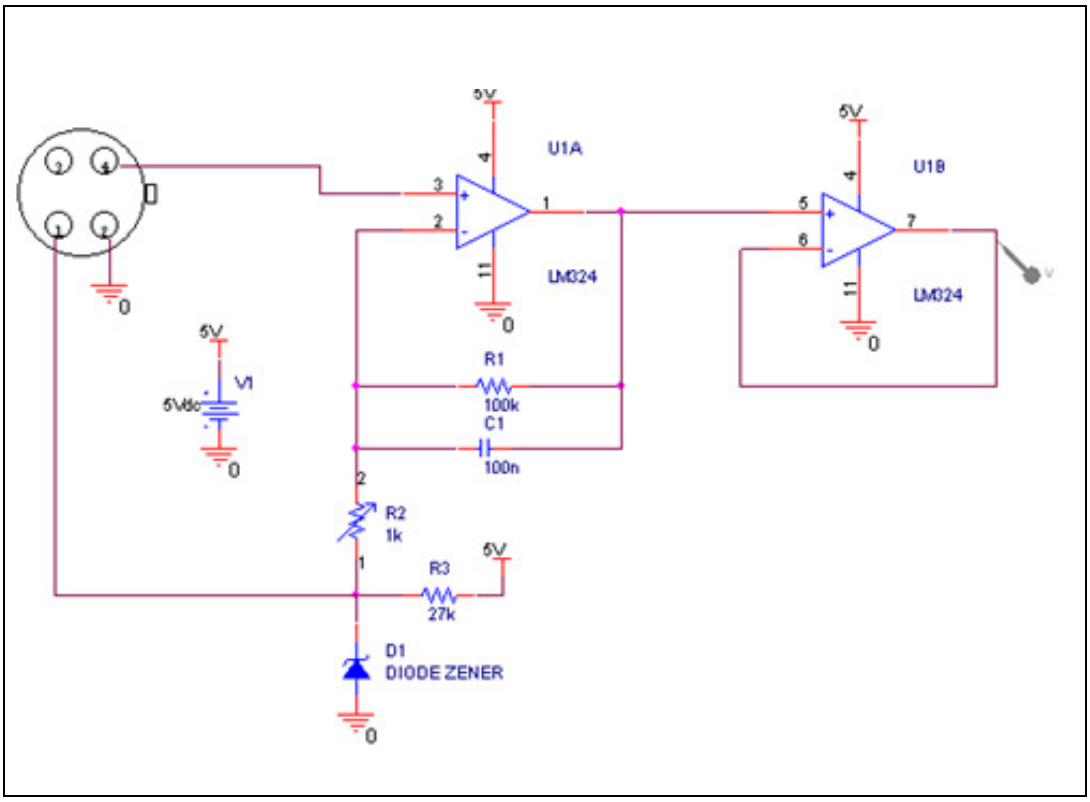

Figure 5.1: The circuit diagram of the modified thermopile sensor circuit for capturing an analog signal

The analog output is digitized by using a PIC16F877A-type microcontroller device and sent to the computer via an RS-232 to USB

converter. Then, the output signal received from the USB port is read from HyperTerminal application and saved to be processed.

The continuous time analog signal is sampled with a sampling frequency, f_s, of 100 Hz and quantized at 8 bits. Typical sampled signals for no-activity case and gas leak event are shown in Figure 5.2. The x-axis in the figures represents the number of samples recorded. Each 100 samples correspond to 1 second. The VOC gas leak, shown in Figure 5.2 (b), is very close to the thermopile sensor (at a distance of 15-20 cm). The most significant property of the sensor output signal is its periodicity. In addition, periods of the signals for no-activity case and gas leak event are different. Frequency of the signal increases with the presence of VOC gas leak in the viewing range of the thermopile sensor.

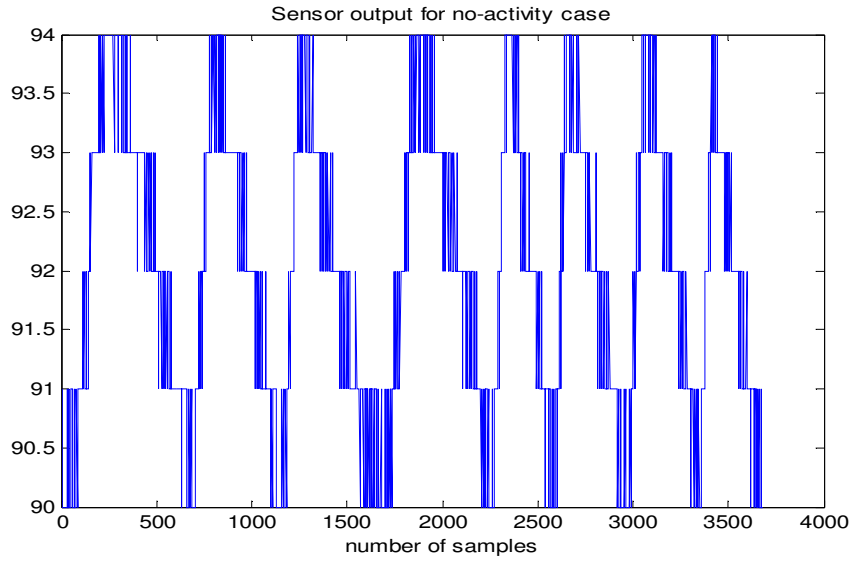

(a)

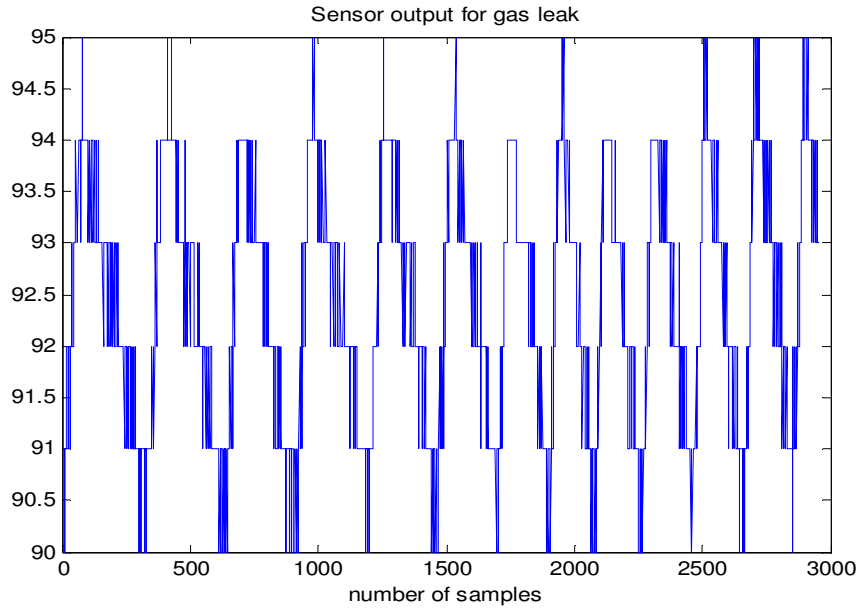

(b)

Figure 5.2: Thermopile sensor output signal for (a) no-activity and (b) VOC gas leak. Sampling frequency is 100 Hz.

5.3 Analysis of Periodic Nature in Signals

In the analysis of the output signal received from the thermopile sensor, one can observe the increase in the frequency of the output signal when there is a VOC gas leak in the viewing range of the thermopile sensor. In Section 5.4, we develop a method for VOC gas leak detection, by using the periods of the sensor output signals for no-activity and gas leak event. We will use the method developed for images in [26], to detect periodic behavior in 1-D signals.

Cutler and Davis [26] describe a technique that detects periodic motion in images. Similarity between images is used to detect and analyze periodicity.

They first segment moving objects from the background and compute the object's self-similarity. The self-similarity metric is periodic for periodic motion and is analyzed in Fourier domain for detection and characterization of periodicity.

In [26], it is assumed that the camera is static, the size and the orientation of the objects of interest do not change apparently during several periods and the frame rate is sufficient to capture the periodic motion. In segmentation of the moving object, it is suggested to first compute a background and then subtract it from the current image. Background is computed by taking the 1-D median for each pixel over the previous N frames (N is between 50 and 200). For subtraction of the background B with the current image I, the following color similarity metric,

$$D(x,y) = \sum_{C \in \{R,G,B\}} |I_c(x,y) - B_c(x,y)| \tag{5.4}$$

is used. The foreground threshold is set to the value $K\ \sigma$, where K is a constant and σ is the average standard deviation of the white noise in the video system for the RGB color channels ($\sigma = 3$ and K is typically 10). Having the foreground, moving objects are tracked by using a template-based tracker.

To detect periodicity, segmented object is first aligned using the object's centroid and resized by using a Mitchell filter to have the same dimensions. Further, the self-similarity of the object O is computed at times t_1 and t_2 and the image similarity metric is:

$$S(t_1,t_2) = \min_{|d_x,d_y| \le r} \sum_{(x,y) \in B_{O_{t_1}}} |O_{t_1}(x+d_x, y+d_y) - O_{t_2}(x,y)| \tag{5.5}$$

r is search radius and is used to account for any errors in tracking. It is stated that *S* is periodic for periodic motions and a similarity plot should be symmetric. In addition, there will be a dark line on the main diagonal and periodic motions will also have dark lines or curves parallel to the diagonal. To determine if the object has a periodic behavior, 1-D power spectrum of $S(t_1, t_2)$ is estimated for a fixed t_1 and all values of t_2. In [26], it is indicated that a periodic motion will show up as peaks in the spectra at the motion's fundamental frequencies and a peak (or peaks) is significant at frequency f_p if, $P(f_p) > \mu_p + K\sigma_p$, where $P(f_p)$ is the power estimate, K is a threshold value (typically 3), μ_p is the mean and σ_p is the standard deviation of P .

To illustrate the analysis of periodic motion, Figure 5.3 is given in [26]. A test sequence is obtained from a walking person. Figure 5.3 (a) is the first image of a 100 image walking sequence. In similarity plot, Figure 5.3 (b), there is a dark line on the main diagonal and there are also dark lines parallel to the diagonal which represent periodic motions. Figure 5.3 (c) shows the power spectrum of similarity. There are two peaks showing the period, one for the swinging arm and the other for legs.

(a)

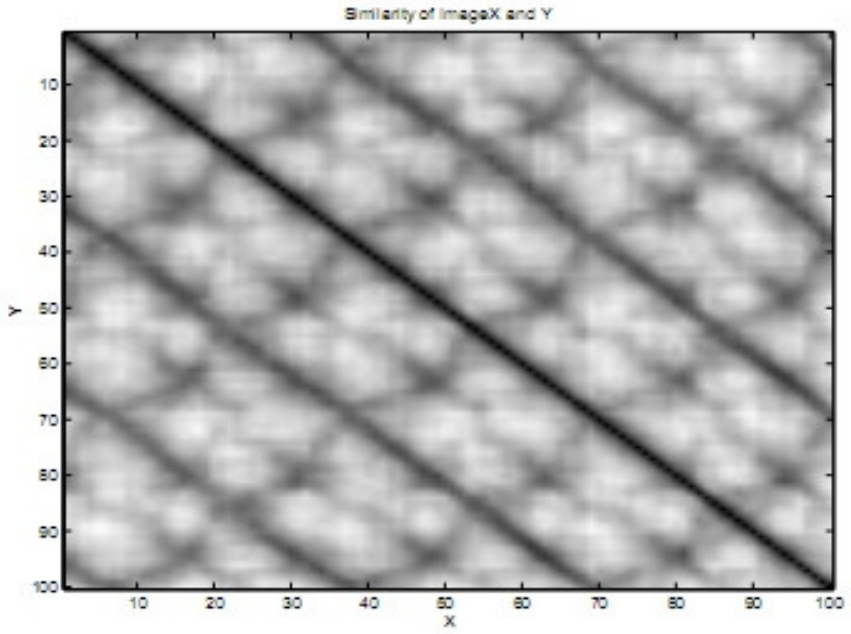

(b)

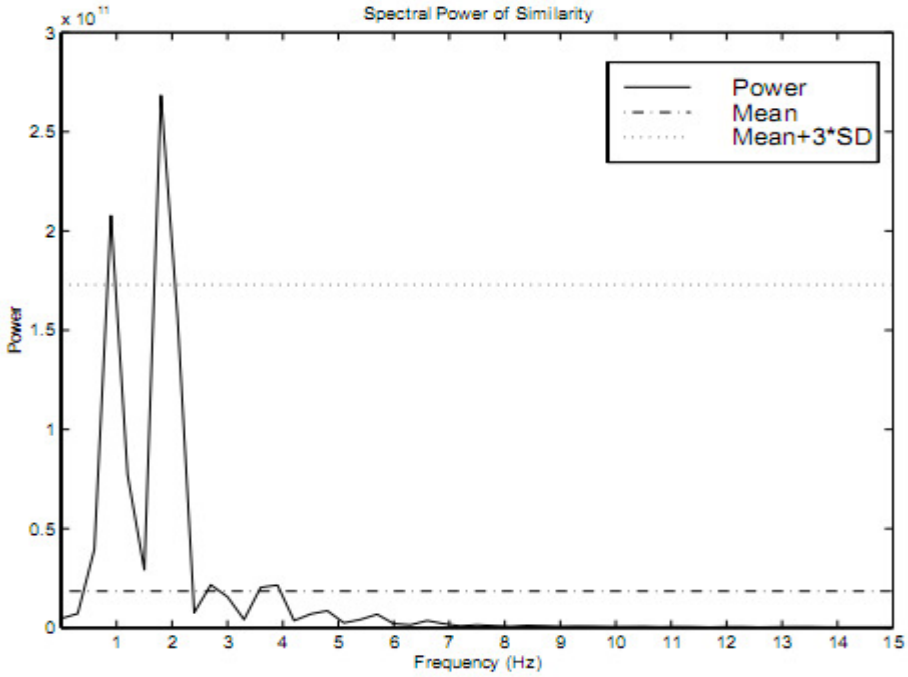

(c)

Figure 5.3: (a) First image of the walking sequence. (b) Walking sequence similarity plot. (c) Average power spectrum of all columns.

5.4 Period-based Analysis of the Sensor Data

The period-based analysis of the thermopile sensor output signal uses the fact that the signal is periodic and the period is different for 'no-activity' and 'gas leak' classes. First, whether the output signal is periodic or not is determined by modifying the method in [26] to 1-D signal case and then the period of each member of each class is found. Section 5.4.1 describes the process to determine whether the signal is periodic or not.

5.4.1 Detection of Periodicity

To determine whether the thermopile output signal is periodic or not, the procedure described in [26] is used with appropriate modifications. A camera is used in [26] and the technique for periodicity detection is introduced accordingly, but the thermopile sensor can be visualized as a single-pixel camera and therefore the periodicity calculation for video image can also be used for the thermopile sensor. A similarity plot and 1-D power spectrum of the output signal is estimated. For periodic motions similarity plot is periodic and a periodic motion shows up as a significant peak in the spectra at a frequency f_p if $P(f_p) > \mu_p + K\sigma_p$, where $P(f_p)$ is the power estimate, K is a threshold value and equals to 3, μ_p is the mean and σ_p is the standard deviation of P.

The output signal is smoothed first by using a sequence of moving average filters. Let the output signal of the sensor be $x[n]$ and $y[n]$ be the smoothed signal. $y[n]$ by using a span of 5 is described as follows [31]:

$$y[n]=\frac{1}{5}(x[n-2]+x[n-1]+x[n]+x[n+1]+x[n+2]) \tag{5.6}$$

Figure 5.4 (a) shows the smoothed sensor signal output for a VOC gas leak, by using a sequence of moving average filters.

Then the difference matrix *m* of *y*[*n*] of length *l* is obtained by using equation (5.2). Consequently, the difference matrix has a size *l x l*. The smoothed output signal *y*[*n*] and the similarity plot for the VOC gas leak shown in Figure 5.2 (b) is presented in Figure 5.4. Similarity plot is symmetric and there is a dark line on the main diagonal with the dark curves parallel to it, which are observed when the signal is periodic.

$$m=\begin{bmatrix} 0 & y(1)-y(2) & y(1)-y(3) & \dots & y(1)-y(l) \\ y(2)-y(1) & 0 & y(2)-y(3) & \dots & y(2)-y(l) \\ y(3)-y(1) & y(3)-y(2) & 0 & \dots & y(3)-y(l) \\ . & . & . & . & . \\ . & . & . & . & . \\ y(l)-y(1) & y(l)-y(2) & y(l)-y(3) & \dots & 0 \end{bmatrix} \tag{5.7}$$

The difference matrix can also be denoted as:

$$m = [c_1 \quad c_2 \quad c_3 \quad \dots \quad c_l] \tag{5.8}$$

Let m_i denote the mean of the column i. m_i's are subtracted from c_i's and absolute value of the difference vector with updated c_i's is taken after a Fast Fourier Transform (FFT). Average power spectrum is obtained by taking the mean of all rows in *m* and is shown in Figure 5.5. The signal has significant peaks where $P(f) > \mu_p + K\,\sigma_p$. Therefore, it is concluded that the sensor output

signal is periodic and a period-based analysis can be carried out for VOC gas detection.

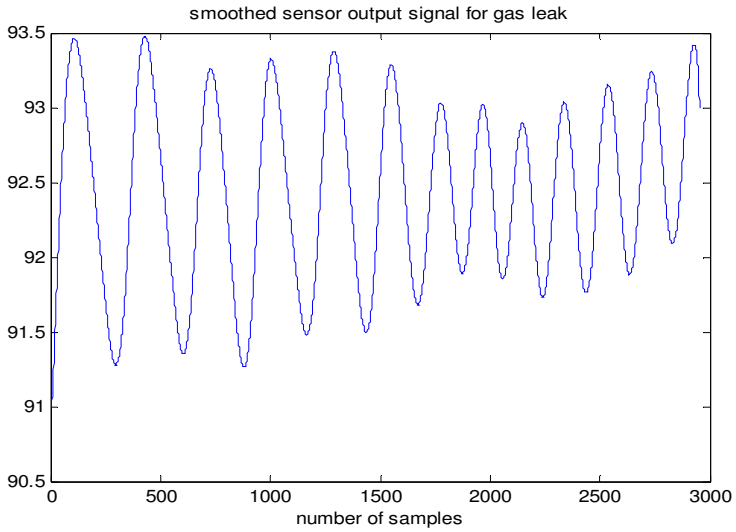

(a)

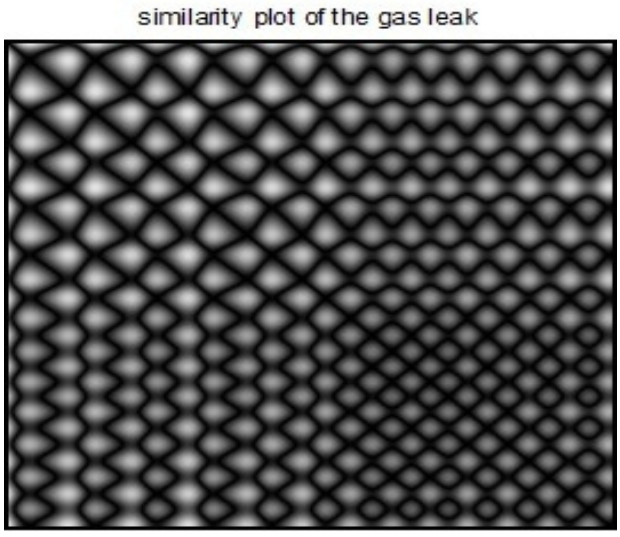

(b)

Figure 5.4: (a) Smoothed output signal using a sequence of moving average filters (b) similarity plot of the VOC gas leak.

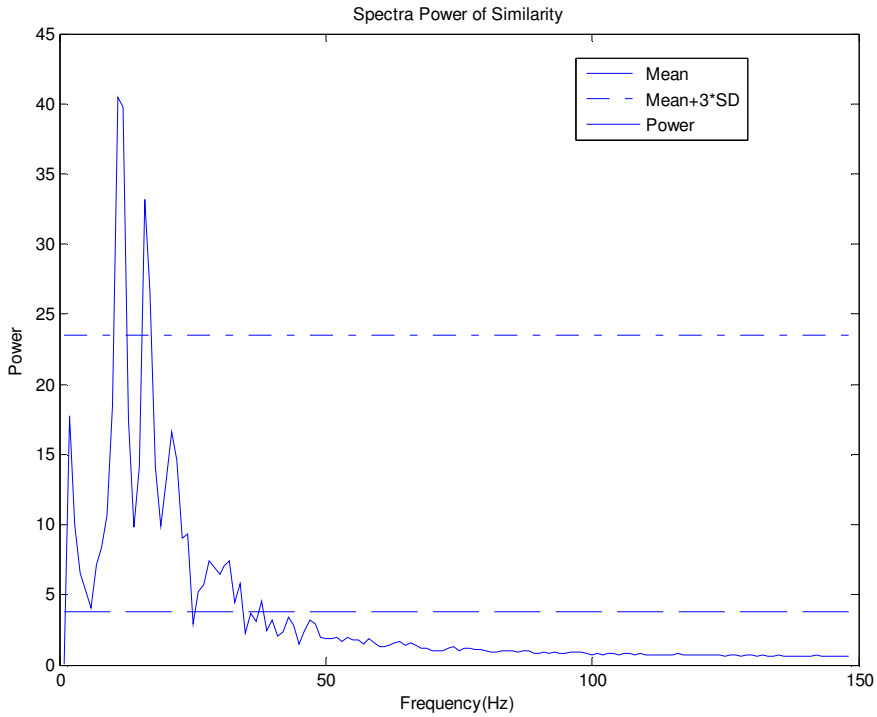

Figure 5.5: Average power spectrum of all columns

5.4.2 Methods of Finding the Period of a Signal

The period of the sensor output signal can be found from the original data by first smoothing the signal and taking the mean of the distances between maxima or minima points, also known as extremas. Extremas are detected as follows: First the difference between subsequent elements are computed and hold in a difference vector. The elements in the difference vector are changed with '1's if they are positive, otherwise with '0's. A positive value means positive slope and a negative value means negative slope. Afterwards, the differences between subsequent elements in the updated difference vector are computed. Let *i* and *j* be the index of the values -1 and +1 in the last difference vector, respectively. Then *i+1* is the index of the maxima point and *j+1* is the

index of the minima point. In the case of flat peaks, which are not common in the sensor output signal, the middle element in the flat peak is detected as extrema. The first and the last detected maxima or minima points are not taken into account in the analysis, because they are always considered as extrema due to the algorithm implemented, however may be not. In this section, alternative methods to find the period are introduced: Average Power Spectrum Method, Average Magnitude Difference Function Method (AMDF), Auto-covariance Method and Co-difference Method.

Average Power Spectrum Method

In this method, the same procedure in Section 5.3 is followed and the average power spectrum of all columns is obtained. Then, the index of the peak that has the maximum value is found. The period is detected by dividing the length of the transformed difference vector by this index.

In the following methods, once the functions are obtained, maxima and minima points are detected and the period is determined accordingly. Functions have the same periods with the original signals.

Average Magnitude Difference Function (AMDF) Method

Average magnitude difference function is a variation on autocorrelation analysis. Instead of correlating the input signal, it forms a difference signal between the original and delayed signal and the absolute magnitude of the difference is taken at each delay [32]. AMDF is defined as:

$$\Psi_y(n) = \frac{1}{N}\sum_{k=0}^{N-1} | y(k) - y(n+k) | \tag{5.9}$$

where N is the length of the signal $y(n)$. $\Psi(n)$ is smoothed by a sequence of moving average filters and the period is determined after the detection of the extremas followed by averaging the distances between each maxima or minima points in terms of number of samples. AMDF of the VOC gas leak in Figure 5.2 (b) is shown in Figure 5.6.

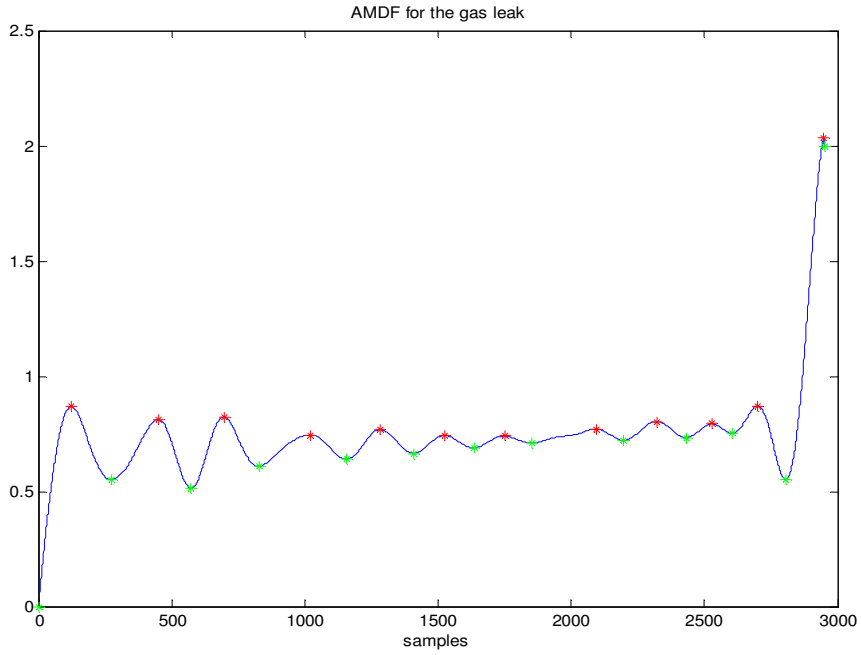

Figure 5.6: Average magnitude difference function for the VOC gas leak

Autocorrelation Method

Autocorrelation is the cross-correlation of a signal with itself [6] and described by:

$$\Phi_y[n] = \frac{1}{N}\sum_{k=0}^{N-1}(y[k]-m_y)(y[n+k]-m_y) \tag{5.10}$$

where N is the length and m_y is the mean of the signal $y[n]$. Maximum similarity occurs when the time shifting is zero and another maximum should occur when the time shifting of the signal corresponds to the fundamental period. Therefore the index of the second maximum is the period of the signal. Autocorrelation function of the VOC gas leak in Figure 5.2 (b) is shown in Figure 5.7.

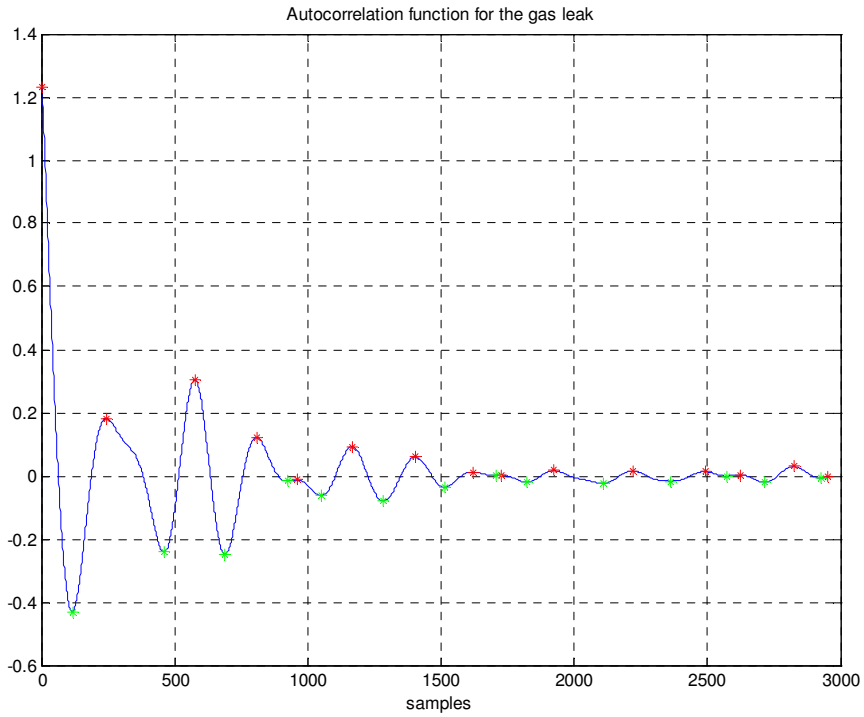

Figure 5.7: Autocorrelation function for the VOC gas leak with marked extrema point

Co-difference Method

A novel technique, Co-difference Method, is described to find the period of a signal. Co-difference function is defined as:

$$\Gamma_y[n] = \frac{1}{N}\sum_{k=0}^{N-1}(y[k]-m_y)\otimes(y[n+k]-m_y) \tag{5.11}$$

where N is the length and m_y is the mean of the signal $y[n]$ and the operator is defined as follows:

$$A \otimes B = \mathrm{sgn}(AB)(|A|+|B|), \tag{5.12}$$

for $A, B \in \Re$. Co-difference function of the VOC gas leak in Figure 5.2 (b) is shown in Figure 5.8. The period of the input signal is equal to the period of its co-difference function and found by using the extrema point analysis.

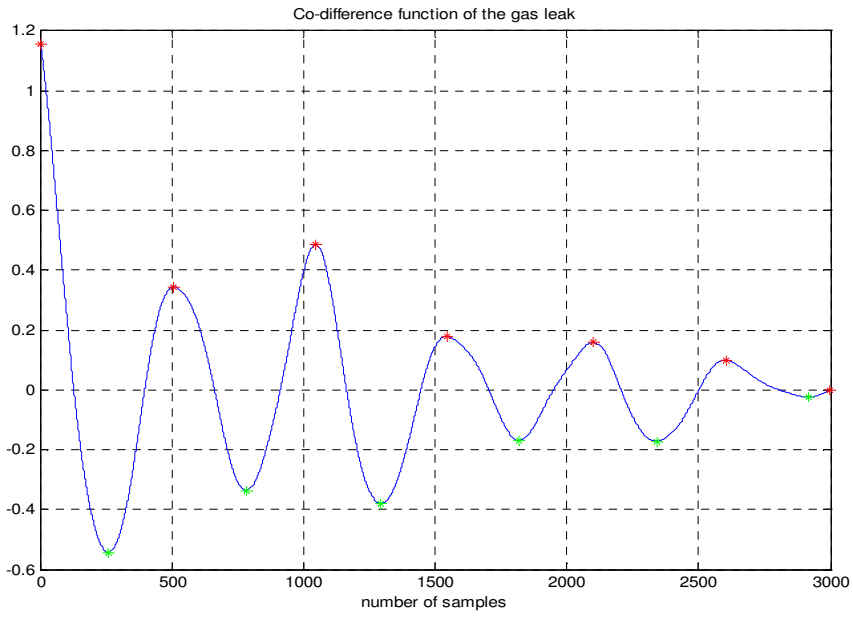

Figure 5.8: Co-difference function of the VOC gas leak with marked extrema points

5.5 HMM-based Analysis of the Sensor Data

The HMM-based analysis is carried out in the wavelet domain. Because, wavelet sub-signals of a waveform are not affected by the slow variations in the environment, which is desired to be so. Let $x[n]$ be a sampled version of the signal coming out of the PIR sensor and $w[k]$ be the wavelet coefficients. Wavelets are obtained after an high pass filtering followed by a dyadic decimation as shown in Figure 5.10. Wavelets of the VOC gas leak are shown in Figure 5.9. While each 100 samples correspond to 1 second in Figure 5.2 (b), in the wavelet domain each 100 samples correspond to 2 seconds, because of downsampling the high-pass filtered signal by a factor of 2.

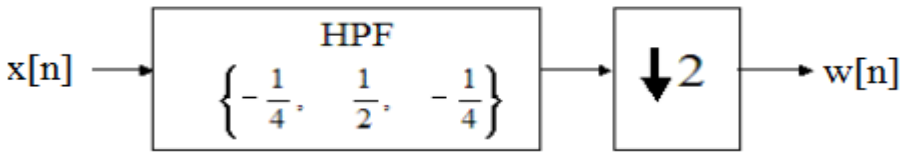

Figure 5.9: Single-stage wavelet filter bank

While applying HMMs on the sensor signal in the wavelet domain, a similar procedure is used with the one in Section 4.3.2. In this case there are two types of events to be classified: no-activity and gas leak. Two threshold values, T_1 and T_2, are defined such that T_1 is negative and T_2 is positive and they are symmetric with respect to the x-axis. Wavelet coefficients of the no-activity event remains between T_1 and T_2. Then the states are introduced accordingly. If $w[n] < T_1$, then state S0; if $T_1 < w[n] < T_2$, then state S_1 and if $w[n] > T_2$, then state S_2 is attained. In no-activity case, the system remains in state S_1.

The next step is to compute state transition sequences for predetermined reference signals. Since each reference signal contains one type of event, the whole signal is of interest in the training step. Let a_{ij} and b_{ij} be the number of transitions from state i to j in the state sequences of the reference signals for the 'gas leak' and the 'no-activity' classes respectively and they can be defined as:

$$a=(a_{00}\, a_{01}\, a_{02}\, a_{10}\, a_{11}\, a_{12}\, a_{20}\, a_{21}\, a_{22}) \tag{5.13}$$

$$b=(b_{00}\, b_{01}\, b_{02}\, b_{10}\, b_{11}\, b_{12}\, b_{20}\, b_{21}\, b_{22}) \tag{5.14}$$

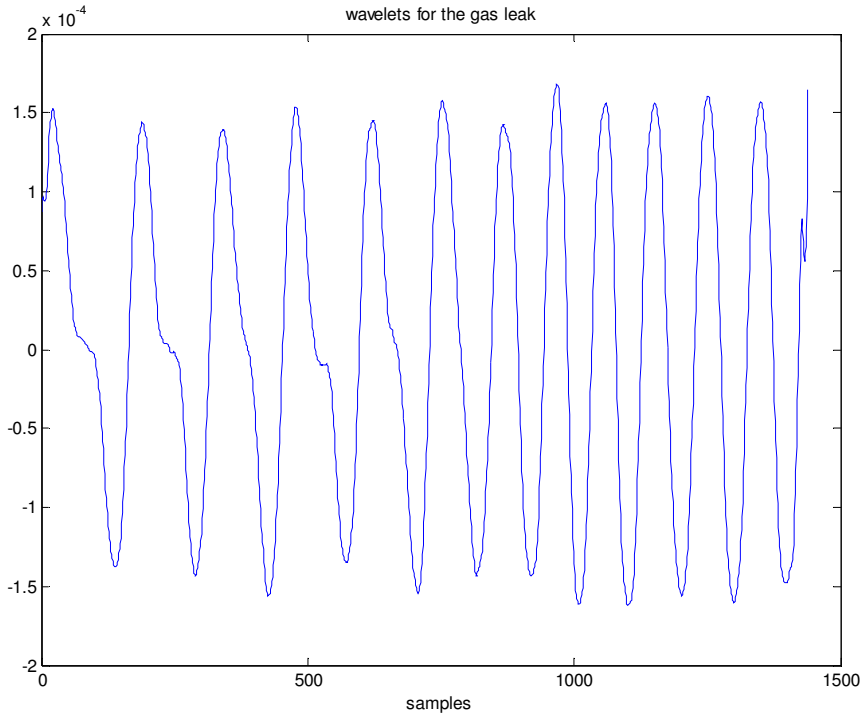

Figure 5.10: Wavelet coefficients of the VOC gas leak in Figure 5.2 (b)

The state diagrams are shown in Figure 4.7. Let the lengths of the reference signals for 'gas leak' and 'no-activity' classes be *L1* and *L2,* respectively. Then the reference probabilities for each transition to occur is:

$$p_a(i,j) = \frac{1}{L_1} a_{ij} \tag{5.15}$$

and

$$p_b(i,j) = \frac{1}{L_2} b_{ij} \tag{5.16}$$

for the 'gas leak' and 'no-activity' classes respectively. For the training of the HMMs, the state transition probabilities are estimated from the wavelet coefficients covering a time frame of 25 seconds. Let t_{ij} be the number of transitions from state i to j for the test signal. Then the probabilities for the state sequence C of belonging to 'gas leak' and 'no-activity' classes are, respectively:

$$P_a(C) = \sum_{i=0}^{2} \sum_{j=0}^{2} t_{ij} \log_{10}(p_a(i,j)) \tag{5.17}$$

and

$$P_b(C) = \sum_{i=0}^{2} \sum_{j=0}^{2} t_{ij} \log_{10}(p_b(i,j)) \tag{5.18}$$

where L is the length of the state sequence C of the test signal. The state sequence C is divided into windows of length 150 and each window is fed into each model. The model that yields the highest probability is determined as the result of the analysis of that window. Each window corresponds to 3 seconds, therefore the result is monitored at each 3 seconds.

5.6 Experimental Results

The sensor output signal is sampled at 100 Hz and quantized at 8 bits. Analysis of the signal is made in MATLAB running on a PC. Digitized output signal is fed to the PC via RS-232 serial port.

We record the VOC gas leak many times at a distance of 15-20 cm away from the sensor. We use a bottled gas, which contains a mixture of butane and propane gases, in ratios %70 and %30 respectively. Experiments are hold in three different rooms and we record only one type of event at each experiment, i.e., no-activity or VOC gas-leak.

In the period-base analysis of the sensor output signal, the period of each test signal is computed. It is noted that the frequency of the signal increases with the VOC gas leak. In other words, the periods of the signals that belong to 'no-activity' class are greater than the ones of 'gas leak' class in general. The classification of events are made by defining a threshold. If the period of the input signal is below that threshold, then we end up with a gas leak, otherwise no-activity in the viewing range of the sensor. 24 experiments are made in total, 8 for each room, and the periods of the sensor output signal that are computed with different methods are presented in Table 5.2. Since the output of the thermopile detector is varying according to the ambient temperature, we define different thresholds for each room. We trigger an alarm if the period of the test signal is below that threshold. VOC gas-leak is successfully detected for all test sequences with an acceptable number of false alarms when there is no-activity. Table 5.3 summarizes the results for 24 test sequences for each method. Except AMDF, the other three methods for finding period have only one false alarm and that occurs as a response to a no-activity test sequence.

		Spectral domain method [26]	AMDF	Auto-correlation method	Co-difference method
Room#1	no-activity#1	500	593	628	637
	no-activity#2	735	880	853	845,5
	no-activity#3	501,66	599,5	436	574,66
	no-activity#4	527,65	553,43	641 ,2	633,3
	gas leak#1	333,28	301,4	348,9	364,57
	gas leak#2	428,57	524,25	519,33	528
	gas leak#3	276	323,87	324	316,16
	gas leak#4	269,09	256,90	205,09	230,63
Room#2	no-activity#1	614,66	501,57	444,41	569,64
	no-activity#2	648,18	629	498,73	590,3
	no-activity#3	1365	802,4	808,55	793,6
	no-activity#4	560	592,71	560,43	571,66
	gas leak#1	605	427,83	326,37	476
	gas leak#2	565	529,28	517,8	542,8
	gas leak#3	387,5	363,71	290,85	423,4
	gas leak#4	483,33	412,39	415	438,4
Room#3	no-activity#1	310,72	322,1	271,34	249,5
	no-activity#2	437,78	490,17	480,33	493,33
	no-activity#3	300,79	272,1	251,23	348,3
	no-activity#4	339,44	356,6	359,53	370,07
	gas leak#1	208,57	219,61	236,294	323,46
	gas leak#2	257,4	201,5	280	227,5
	gas leak#3	267,83	253,68	240,044	256,73
	gas leak#4	247,27	233,22	269,125	230

Table 5.2: Periods of the test sequences, that belong to no-activity and VOC gas leak classes, computed by different methods

			No. of sequences	No. of False Alarms	No. of Alarms
Room#1	Spectral domain method [26]	gas-leak test sequences	4	0	4
		no-activity test sequences	4	0	0
	AMDF	gas-leak test sequences	4	0	4
		no-activity test sequences	4	0	0
	Auto-correlation	gas-leak test sequences	4	0	4
		no-activity test sequences	4	1	1
	Co-difference	gas-leak test sequences	4	0	4
		no-activity test sequences	4	0	0
Room#2	Spectral domain method [26]	gas-leak test sequences	4	0	4
		no-activity test sequences	4	1	1
	AMDF	gas-leak test sequences	4	0	4
		no-activity test sequences	4	1	1
	Auto-correlation	gas-leak test sequences	4	0	0
		no-activity test sequences	4	2	2
	Co-difference	gas-leak test sequences	4	0	4
		no-activity test sequences	4	0	0

Table 5.3: Results for 12 VOC gas leak and 12 no-activity test sequences for different methods. The system triggers an alarm when VOC gas leak is detected.

			No. of Sequences	No. of False Alarms	No. of Alarms
Room#3	Spectral domain method [26]	gas-leak test sequences	4	0	4
		no-activity test sequences	4	0	0
	AMDF	gas-leak test sequences	4	0	4
		no-activity test sequences	4	0	0
	Autocorrelation	gas-leak test sequences	4	0	4
		no-activity test sequences	4	2	2
	Co-difference	gas-leak test sequences	4	0	4
		no-activity test sequences	4	1	1

Table 5.3: Results for 12 VOC gas leak and 12 no-activity test sequences for different methods. The system triggers an alarm when VOC gas leak is detected.

In the HMM-based analysis, we test each sequence by a predetermined model for each room and the same thresholds, $T_1 = -0.5x10^{-4}$ and $T_2 = 0.5x10^{-4}$, are used both for training and the test sequences. Each test sequence is divided into windows of length 150, covering a 3 seconds-time frame. The result of the analysis of each window is hold. If the result of the analysis of two consequent frames is both the gas leak, then the system triggers an alarm. Our method successfully detect the VOC gas leak in room 1. In rooms 2 and 3, VOC gas leak is successfully detected also, but there is a false alarm when there is no activity in the viewing range of the thermopile sensor. Table 5.4 presents the results of the HMM-based analysis of the sensor output.

		No. of Sequences	No. of False Alarms	No. of Alarms
Room#1	Gas Test Sequences	4	0	4
	No-activity Sequences	4	0	0
Room#2	Gas Test Sequences	4	0	4
	No-activity Sequences	4	1	1
Room#3	Gas Test Sequences	4	0	4
	No-activity Sequences	4	1	1

Table 5.4: Classification results of the HMM-based analysis for 12 VOC gas leak and 12 no-activity test sequences

Chapter 6

Conclusion and Future Work

In this study, we proposed and implemented novel and cost efficient methods for VOC gas detection by using a passive infrared sensor and a thermopile sensor. We used the fact that the sensors have spectral responses in the infrared part of the spectrum intersecting with the absorption bands of butane and propane gases. Gases spread out gradually, whereas the IR radiation propagation is very rapid. Therefore, unlike conventional detectors, infrared and thermopile detectors have fast response time. For example, a ME-O2 electrochemical gas sensor has a response time of about 30 seconds [33], a MQ-4 gas sensor has a response time longer than 5 minutes [34] and a hydrogen-selective gas sensor described in [35] has a response time of 50 seconds. On the other hand, we can detect a gas leak with a PIR sensor at 8 seconds and with a thermopile sensor at 6 seconds. Moreover, since the output voltage of the PIR sensor depends on the amount of radiation, it is sufficient for VOC gas leaks to be in the viewing range of the sensor. This provides the means that PIR sensors can be used in large rooms and open areas. But, the thermopile sensor can detect a gas leak in a close vicinity and therefore it can be used only in gas chambers.

We extended the view-based analysis and detection of periodic motion to detection of periodicity of the thermopile sensor output signal. Periodicity is detected from the properties of similarity image and spectral power of similarity. We implemented different methods to determine the period of a periodic signal. We also presented a novel method, Co-difference method, to determine the period of a signal.

In this thesis, we used Markov models which are tailored for VOC gas detection. HMMs were applied on the wavelet transformed data. It is computationally efficient to use wavelet transform in the analysis of the sensor data.

Each type of sensor has its own advantages and disadvantages. With HMMs, as a classification method, we successfully distinguished gas leak from a walking man in analysis of PIR sensor signal. Besides, the thermopile sensor has no spectral response for the wavelengths above 4.21 μm. Consequently, both sensors are functional where people live. On the other hand, it becomes harder for the sensors to detect gas leaks at a long distance. Because, the output voltages become insufficiently low at long distances. Furthermore, the output signal of thermopile sensors highly depends on the temperature changes. Therefore, it is necessary to define appropriate thresholds for period-base analysis and generate appropriate Markov models for each specific place.

As a future work, output signal of the thermopile sensor may be compensated and calibrated by using the reference channel against the changes in the temperature. In this manner, it can be used in everywhere without being updated. Moreover, PIR sensor may be used with a lens that has an IR

transmission range, which can be chosen to be sensitive to a specific gas radiation. The lens may provide better focusing and better results for detection.

Bibliography

[1] "What is Natural Gas?." `http://www.naturalgas.org/overview/background.asp`, Accessed at May 2009.

[2] S. Jurgen, "Remote temperature measurement with perkinelmer thermopile sensors (pyrometry) a practical guide to quantitative results."

[3] J. G. Crowder, S. D. Smith, A. Vass, and J. Keddie, *Mid-infrared Semiconductor Optoelectronics*, ch. Infrared Methods for Gas Detection, pp. 595–613. Springer Berlin / Heidelberg, 2006.

[4] B. Töreyin, E. Soyer, O. Urfalioglu, and A. Cetin, "Flame Detection System Based on Wavelet Analysis of PIR Sensor Signals with an HMM Decision Mechanism," in *16th European Signal Processing Conference (EUSIPCO 2008)*, 2008.

[5] N. Yoshiike, K. Morinaka, K. Hashimoto, M. Kawaguri, and S. Tanaka, "360° direction type human information sensor," *Sensors and Actuators A: Physical*, vol. 77, no. 3, pp. 199 – 208, 1999.

[6] T. Hussain, A. Baig, T. Saadawi, and S. Ahmed, "Infrared pyroelectric sensor for detection of vehicular traffic using digital signal processing techniques," *Vehicular Technology, IEEE Transactions on*, vol. 44, pp. 683–689, Aug 1995.

[7] Cambridge Sensotec, "Gas analysis methods." `http://pdf.directindustry.com/pdf/cambridge-sensotec/`

gas-detection-methods-explained/14678-44117-42.html, Accessed at May 2009.

[8] Wikipedia, "Gas leak detection — wikipedia, the free encyclopedia," 2009. [Online; accessed 12-January-2009].

[9] C. F. Tsai and M. S. Young, "Pyroelectric infrared sensor-based thermometer for monitoring indoor objects," *Review of Scientific Instruments*, vol. 74, no. 12, pp. 5267–5273, 2003.

[10] K. N. Ha, K. C. Lee, and S. Lee, "Development of pir sensor based indoor location detection system for smart home," in *SICE-ICASE, 2006. International Joint Conference*, pp. 2162–2167, Oct. 2006.

[11] O. Urfaliglu, E. Soyer, B. Toreyin, and A. Cetin, "Pir-sensor based human motion event classification," in *Signal Processing, Communication and Applications Conference, 2008. SIU 2008. IEEE 16th*, pp. 1–4, April 2008.

[12] W. Lee, "Method and apparatus for detecting direction and speed using pir sensor," March 1994.

[13] P. T. Moseley, "Solid state gas sensors," *Measurement Science and Technology*, vol. 8, no. 3, p. 223, 1997.

[14] J. E. Tozier, A. Anouchi, and R. Critchlow, "Constant temperature catalytic gas detection instrument," September 1985.

[15] I. Simon and M. Arndt, "Thermal and gas-sensing properties of a micromachined thermal conductivity sensor for the detection of hydrogen in automotive applications," *Sensors and Actuators A: Physical*, vol. 97-98, pp. 104 – 108, 2002.

[16] D.D. Lee and D.S. Lee, "Environmental gas sensors," *Sensors Journal, IEEE*, vol. 1, pp. 214–224, Oct 2001.

[17] Figaro Engineering Inc., "Tgs 2610 - for the detection of lp gas."

[18] E. Bakker and M. Telting-Diaz, "Electrochemical sensors," *Anal. Chem.*, vol. 74, 2002.

[19] N. Aschenbrenner, "Laser diode measures carbon monoxide traces." `http://w1.siemens.com/innovation/en/news_events/ct_pressemitteilungen/index/e_research_news/2009/e_22_resnews_0901_1.htm`, Accessed at May 2009.

[20] S. Kay, *Intuitive Probability and Random Processes using MATLAB*. Secaucus, NJ, USA: Springer-Verlag New York, Inc., 2007.

[21] L. R. Rabiner and B. H. Juang, "An introduction to hidden Markov models," *IEEE ASSP Magazine*, vol. 3, pp. 4–16, Jan 1986.

[22] C. Kereliuk, "An introduction to hmms." `http://www.music.mcgill.ca/corey/mumt611/assign3/Kereliuk07HiddenMarkov.pdf`, Accessed at May 2009.

[23] Glolab Corporation, "Infrared parts manual pir325 fl65," 2003.

[24] Y. Y. Tan, *Wavelet Theory and Its Application to Pattern Recognition (Machine Perception & Artificial Intelligence)*. World Scientific Publishing Company.

[25] D. B. Percival and A. T. Walden, *Wavelet Methods for Time Series Analysis (Cambridge Series in Statistical and Probabilistic Mathematics)*. Cambridge University Press, February 2000.

[26] R. Cutler and L. Davis, "View-based detection and analysis of periodic motion," in *In International Conference on Patern Recognition*, pp. 1–4, 1998.

[27] S. Middelhoek, "Silicon sensors," *Measurement Science and Technology*, vol. 6, no. 12, p. 1641, 1995.

[28] A. W. Herwaarden, D. Duyn, and B. W. Oudheusden, "Integrated thermopile sensors," *Sensors and Actuators*, vol. 21, pp. 621–630, 1989.

[29] HEIMANN Sensor GmbH, "Datasheet heimann sensor integrated module to-case for gas detection co2 - type his a21 f4.26 4pin," 2005.

[30] Q. Tan, W. Zhang, C. Xue, J. Xiong, Y. Ma, and F. Wen, "Design of mini-multi-gas monitoring system based on IR absorption," *Optics Laser Technology*, vol. 40, pp. 703–710, July 2008.

[31] A. Gersho and R. M. Gray, *Vector quantization and signal compression*. Norwell, MA, USA: Kluwer Academic Publishers, 1991.

[32] M. Ross, H. Shaffer, A. Cohen, R. Freudberg, and H. Manley, "Average magnitude difference function pitch extractor," *Acoustics, Speech and Signal Processing, IEEE Transactions on*, vol. 22, pp. 353–362, Oct 1974.

[33] Hanwei Electronics, "ME-O2 Electrochemical Gas Sensor." `http://www.diytrade.com/china/4/products/5010173/O2_electrochemical_gas_sensors.html`, Accessed at May 2009.

[34] Hanwei Electronics, "Technical Data MQ4 Gas Sensor." `http://www.hwsensor.com/English/PDF/sensor/MQ-4.pdf`, Accessed at May 2009.

[35] W. Shin, M. Matsumiya, N. Izu, and N. Murayama, "Hydrogen-selective thermoelectric gas sensor," *Sensors and Actuators B: Chemical*, vol. 93, no. 1-3, pp. 304 – 308, 2003. Proceedings of the Ninth International Meeting on Chemical Sensors.